# Mass Budgeting for Hybrid Rocket Engines Optimization

December 2022

## POLITECNICO DI TORINO

Master's Degree Thesis

Master's Degree in Aerospace Engineering


Politecnico di Torino

Supervisor Prof. Filippo MASSENI  Candidate Nicola MELONI

**Abstract**

This Thesis work focuses on the optimization of engine design and trajectory for Hybrid Rocket Engines (HREs). In particular, the optimal choices of tank geometry and material are analyzed. HREs are well suited for many applications, among which small satellite launchers are here considered.
In this Thesis work, each stage of a three-stage launcher is equipped with the same hybrid rocket engines, organized in different numbers: six, three, and one respectively in the first, second and third stage, in order to minimize the costs by means of a high system commonality. A simple blow-down feed system and an airborne launch are taken into account.
First, the optimization process compares the launcher performance for several engine geometries and materials, to find out the best couple aiming at the maximization of the payload mass for a reference engine design point. In this way, a kind of Database is created to group these several scenarios and, through a comparison of them, the best match is selected. At this point, the real optimization process begins: the optimization procedure fixes one by one the couple of geometry-material and optimizes the engine design by adjusting the design parameters, which are the initial mixture ratio and the initial pressurizing gas volume in this application. A direct method optimizes the engine design, while an indirect procedure evaluates and optimizes the corresponding ascent trajectory.
Once this process is completed for all geometry-material couples, a new database is created and the optimal couple is found, together with the corresponding optimal engine design and trajectory.
The information collected in the databases could be useful in future works on the same or analogous topic to lead an early design phase, because of the functional relationship established between geometries, materials and engine designs.

Questo lavoro di tesi si concentra sull'ottimizzazione del design del motore e della traiettoria per Endoreattori a Propellenti Ibridi (HREs). Nello specifico, viene analizzata la scelta ottimale di materiale e geometria del serbatoio. Gli HREs sono adatti a diverse applicazioni tra cui quelle per piccoli lanciatori di satelliti, qui considerati.
In questo lavoro di tesi, ogni stadio del lanciatore tri-stadio è equipaggiato con i medesimi motori a razzo a propellente ibrido organizzati in differente numero: sei, tre e uno rispettivamente per il primo, secondo e terzo stadio, così da minimizzare i costi per mezzo di un'elevata comunanza di sistema. Vengono presi in considerazione un semplice sistema di alimentazione blow-down e un lancio aereo.
Nella fase iniziale, il processo di ottimizzazione consiste nel confrontare le performance del lanciatore per diverse geometrie e materiali del motore, per trovare la migliore coppia che mira alla massimizzazione della massa del carico utile per un punto di progettazione del motore di riferimento. In questo modo, una sorta di database viene creato per raggruppare questi diversi scenari e, tramite un confronto di questi, selezionare la miglior coppia. A questo punto inizia il vero processo di ottimizzazione: la procedura di ottimizzazione consiste nel fissare una per una le coppie geometria-materiale and ottimizzare il design del motore cambiando i parametri di design, che sono il rapporto di miscela iniziale (mixture ratio) e il volume del gas pressurizzante (ullage volume). L'ottimizzazione del design del motore viene fatta con un metodo diretto, mentre una procedura indiretta valuta ed ottimizza la corrispondente traiettoria di ascesa.
Una volta che questo processo è completato per tutte le coppie geometria-materiale, viene creato un nuovo database e viene trovata la coppia ottimale, insieme al corrispettivo design ottimale del motore e la traiettoria.
Le informazioni raccolte nei database potrebbero essere utili, per ricerche future relative allo stesso o a simili argomenti, per guidare una prima fase di design, grazie alle relazioni funzionali definite tra geometrie, materiali e design del motore.

# Acknowledgments

Prima di procedere con la trattazione, vorrei dedicare qualche riga a tutti coloro che mi sono stati vicini in questo percorso di crescita personale e professionale.
Un sentito ringraziamento al mio relatore, il Professor F. Masseni per la sua infinita disponibilità e tempestività rispetto ad ogni mio dubbio o richiesta. La ringrazio per avermi fornito tutto il materiale necessario alla stesura e allo sviluppo dell'elaborato. Inoltre, la ringrazio per la puntualità e precisione nelle spiegazioni, tramite cui ho potuto aumentare il mio bagaglio culturale su argomenti a me cari, quali sono quelli relativi agli Endoreattori.

Un ringraziamento speciale va alla mia famiglia. A mia madre Serena, per la sua dolcezza e gentilezza costante, che hanno reso i momenti più difficili un po' più facili da affrontare. A mio padre Carlo, duro fuori ma morbido dentro. Grazie perché ogni nostra chiacchierata, discussione o confronto, mi ha reso l'uomo che sono oggi. Al mio fratellino Fabio, a cui spero di riuscire a dare almeno la metà dell'aiuto e del supporto che lui da a me.
Tutti i traguardi che ho realizzato in vita mia e tutti quelli che realizzerò sono anche vostri e per questo non vi sarò mai grato abbastanza.

A Beatrice. Ogni mio pensiero, dubbio o problema assume una sfumatura diversa se affrontato con te, e tutto diventa possibile. Grazie per essermi sempre vicina e per essere parte della mia vita. Questo risultato è anche tuo, poiché il tuo supporto è fondamentale ogni giorno.

«Sei il sogno che comincia nel momento in cui mi sveglio»,

Articolo 31

Grazie a Riccardo, non tutti i fratelli nascono dalla stessa madre, e tu ne sei la prova. Grazie per tutte le sere passate a chiacchierare, hanno reso la mia vita più leggera e divertente.
Ad Alessandro, a Bianca ed a tutti gli altri amici da una vita, senza la vostra preziosa amicizia il mondo sarebbe più grigio.
A Marco, Simone, Carlo, Dario e Luca, coinquilini vecchi e nuovi che ieri come oggi mi fanno sentire a casa come se fossimo una vera famiglia.

Infine, un ringraziamento va a me stesso per averci creduto sempre anche quando sembrava impossibile.

«A man's dream will never die»,

Echiro Oda (Marshall D. Teach)

# Contents

# List of Tables

# List of Figures

# 1 Introduction

In this first thesis chapter, some aspects of rocket engines will be analysed. Specifically, a short overview of performance and types of the existing rockets will be done, with a particular focus on HRE, their propellant, performance and their operating principle. Finally, advantages, disadvantages and related performance improvement solutions will be presented. The definitions presented later are mainly based on the work of Sutton & Biblarz, contained in the book "Rocket Propulsion Elements" [1], to which the personal notes taken during Professor D. Pastrone's [2] course have been integrated.

## 1.1 General concept

### 1.1.1 Performance and basis principle

Before starting with an overview of the rocket, the main physical quantities that lead the operations of the latter are explained in order to make the following section clearer and easier to understand.

- Thrust: usually indicated with $F$ and measured in N or kN, can be calculated in an easy way like

$$F = \dot{m} w_e + A_e(p_e - p_0) \tag{1}$$

  where $\dot{m}$ is the rocket engine mass flow, $w_e$ is the exit velocity, $A_e$ is the nozzle exit area, $p_e$ the pressure in the same zone and $p_0$ the ambient pressure (if it is the case of complete vacuum $p_0 = 0$) [1].

- Thrust coefficient: indicated with $C_F$, is an adimensional number with the role of taking into account the difference and the improvement of the thrust obtained by the rocket engine with the contribution of the nozzle and the thrust obtained using only a combustion chamber perforated in the back

$$C_F = \frac{F}{p_c A_t} \tag{2}$$

  where $p_c$ is the chamber pressure and $A_t$ is the nozzle throat area. Using a more accurate equation about the thrust the expansion term appears. So, in short, this coefficient describes the nozzle expansion property [1].

- Characteristic velocity: indicated with $c^*$ is defined in the following way

$$c^* = \frac{p_c A_t}{\dot{m}} \tag{3}$$

  This quantities is not a physical velocity, however, is used for comparing the relative performance of different chemical rocket systems and propellants [1].

- Effective exhaust velocity: indicated with $c$, is defined as

$$c = \frac{F}{\dot{m}} = C_F \bullet c^* \tag{4}$$

  The effective exhaust velocity represents an average or mass-equivalent speed at which propellant is being ejected from the rocket engine. Moreover, $c$ and $I_s$ only differ by a constant $g_0$, either one can be used in order to measure the performance of the rocket [1].

- Total impulse: indicated with

$$I_t = \int_{t_0}^{t_f} F dt \tag{5}$$

  is measured in $N \bullet s$. $t_0$ and $t_f$ are respectively the start and the shutdown of the rocket engine [1].

- Specific impulse: indicated with $I_s$, it is misured in $s$ and defined as

$$I_s = \frac{I_t}{g_0 M_P} = \frac{c}{g_0} \tag{6}$$

  where $g_0$ is the gravity acceleration and $M_P$ is the propellant specific mass stored on board .
  $I_s$, if the thrust is considered constant and considerable equal to $g_0 M_P$, is exactly the operating time of the rocket engine [1]

$$I_s = \Delta t = t_f - t_0 \tag{7}$$

- Mixture ratio: indicated with $\alpha$, it is an adimensional number that indicates the proportion between quantities of oxidant and fuel during the combustion process in the rocket engine combustion chamber [1]

$$\alpha = \frac{\dot{m}_{ox}}{\dot{m}_{fuel}} \tag{8}$$

- Density specific impulse: indicated with $I_\rho$, it is measured in $\frac{kg \bullet s}{m^3}$. This quantity means the volume of the propellant consumed for every second of the rocket engine working, in order to obtain a determined level of thrust [1]

$$I_\rho = I_s \rho \tag{9}$$

where $\rho$ is

$$\rho = \frac{\rho_o \rho_f (1 + MR)}{MR \bullet \rho_f + \rho_o} \tag{10}$$

So, $\rho$ is the average density calculated with MR. Propellant with $I_\rho$ higher than others show fewer tanks dimension and consequently less weight [1].

### 1.1.2 Tsiolkowsky equation

Ciolkovskij equation, formulated by the Russian intellectual Ciolkovskij (usually known according to the Anglo-Saxon transliteration as Tsiolkovsky), is based on the conservation of momentum, and this equation states that a body can accelerate by ejecting a part of its mass in the opposite direction to that of motion (the direction of the velocity vector).
The classic formulation is

$$\Delta v = c \bullet ln\left(\frac{m_i}{m_f}\right) = I_s g_0 \bullet ln\left(\frac{m_i}{m_f}\right) \tag{11}$$

where $\Delta v$ is the speed increment necessary for a generic manoeuvre, $c$ is the effective exhaust velocity, and $m_i$and $m_f$ are respectively the initial and final mass of the rocket [2].
This equation turns out to be correct only if some hypotheses are satisfied:

1. The effective exhaust velocity $c$, the rocket engine mass flow $\dot{m}$ and the thrust $F$ are all constant during the lift-off phase of the rocket;
2. Total vacuum ambient condition, so the aerodynamical drag is equal to zero $D = 0$;
3. The thrust vector is aligned with the direction of the velocity vector;
4. The thrust is the only external force acting on the rocket.

## 1.2 Rockets classification

Rockets can be divided considering the energy source or the propellant acceleration. The first case includes chemical, nuclear, solar energy etc. In the field of chemical energy, propellants are used in three different ways.
In the first one, there isn't changing in composition; in the second case the propellants are used after decomposition: this is the case of monopropellants like hydrazine and its compounds. This kind of monopropellant, through the combination of a catalyst, undergoes exothermic decomposition producing the heated gas necessary to generate thrust; finally, the last case is that after the chemical reaction: about this case, is necessary to distinguish between the fuel and the oxidant that react to produce a large quantity of energy. This energy allows producing a very high thrust.
Both in the second and third cases is necessary to distinguish between propellant (stored before the reaction) from reaction products.

The last category, according to the propellant state, can be divided into three sub-categories [1]:

1. **Solid Rocket Motors (SRMs)**:
   both oxidant and fuel are stored in the solid phase. They can be stored and mixed in a solid grain, usually cylindrical, with a hole in the middle.

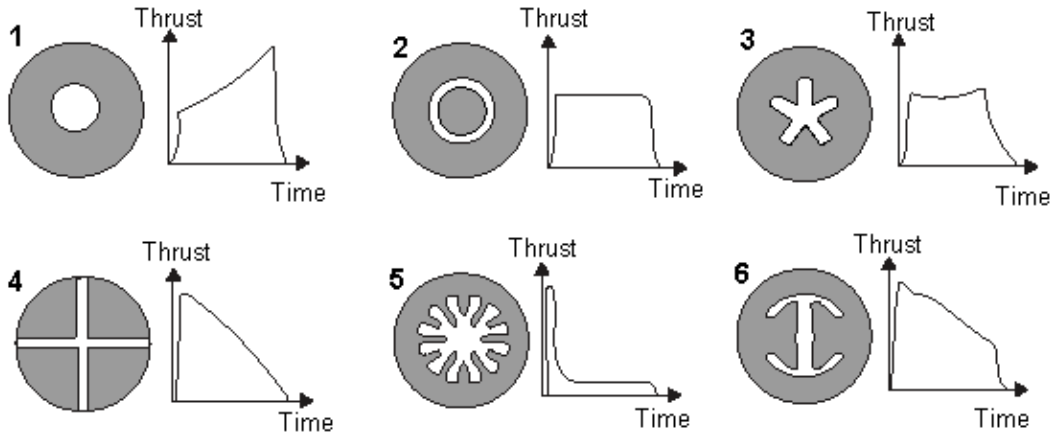


Figure 1: Different grain geometries and their thrust profiles.

The grain forms both the tank and the combustion chamber; a real combustion chamber doesn't exist because the combustion appends only into the grain's hole in the axial direction. Specifically, an electrically activated igniter is needed to start combustion; the propellant grain starts to burn on all its exposed inner surfaces: the grain configuration depends on the mission and can have slots, grooves, holes, or other geometric features that alter the initial burning surface and that determine both initial mass flow rate and the initial thrust [1].
Hot combustion gases flow along the port inside the cavity toward the nozzle. Thus, the combustion chamber is the case, which is a pressure vessel made of metal or fibre-reinforced plastic material. For this reason, the feed system is not present and the propellant turns out to be $82 - 94\%$ of the total rocket engine mass. An insulation layer is present to protect the motor case. This kind of structure makes SRMs relatively simple.
Another feature is the high thrust/weight ratio and the thrust profile can be tailored to specific needs through the grain design, but the engine can't be throttled once ignited. Other disadvantages are that this rocket engine can't be restarted and also no testing or flight check can be done, because of the propellant phase [1].
For this reason, SRMs are mainly used for large boosters, like Space Shuttle and Atlas-V, during the early stages of the flight mission. About SRMs propellants, they can be classified as Homogeneous, where oxidizer and fuel are bonded at a molecular level, and Composite where the bond between oxidizer and fuel is mechanical. Homogeneous propellants are based on Nitrocellulose (NC) and Nitroglycerin(NG), while composite propellants are mainly perchlorates and polymers. Also, additives are used to change chemical, physical and mechanical properties and ballistic behaviour [1].
Lately, fewer and fewer SRMs are used to the detriment of HREs. This is for two reasons:

- Despite structural materials for motor cases and nozzles continuing to be improved, the high-energy propellants appear to be near their limits.

- SRMs are very harmful to the environment: indeed, after several launches (one of these was the space shuttle) are observed some phenomena. For example, The massive cloud generated during liftoff contained rather reactive chemicals such as hydrochloric acid and aluminium oxide. These substances got mixed up with water from the deluge system that cooled down the launch pad and the rocket. This cloud then spread in the surrounding environment, affecting soil and water quality, and damaging vegetation. Also, large amounts of dead fish were found in nearby water bodies. For these environmental reasons, SRMs are being used less and less, while HREs aim to replace them thanks to their greater eco-sustainability.

Figure 2: Inside NASA's Solid Rocket Booster for the Space Launch System Artemis program.

2. **Liquid Rocket Engines (LREs)**:
in this second case, both oxidant and fuel are stored in the liquid phase in two different tanks. These kinds of rockets are more complex than SRMs and are made up of tanks, a control and feed system, the main combustion chamber and the nozzle.
The main features are the possibility of throttling and the ability to switch off and on again. Consequently, these kinds of rockets are used in situations in which throttling is mandatory, like the interplanetary mission or particular types of manoeuvres such as dock, station keeping, etc.
About propellants, the most common oxidizers are LOX (cryogenic liquid oxygen), NTO (nitrogen oxides, like N2O4) and HP (hydrogen peroxide), while the most common fuels are LH2 (cryogenic liquid hydrogen), RP-1 (rocket propellant-1, a very refined type of kerosene, typical of rocket engines) and CH4 (cryogenic methane) [2].
At present, we ordinarily use three liquid bipropellant combinations [2]:

   - The cryogenic oxygen–hydrogen propellant system, used in upper stages and sometimes booster stages of space launch vehicles, gives the highest specific impulse nontoxic propellant combination and one that is best for high vehicle velocity missions.
   - The liquid oxygen, hydrocarbon propellant combination, used for booster stages (and a few second stages) of space launch vehicles, having a higher average density allows more compact booster stages with less inert mass when compared to the previous combination;
   - Not a single bipropellant combination but several ambient temperature storable propellant combinations used in large rocket engines for the first and second stages of ballistic missiles and almost all bipropellant low-thrust, auxiliary or reaction control rocket engines; these allow for long-term storage and almost instant readiness (starting without the delays and the precautions that come with cryogenic propellants).

   Although there are several hazard categories, they do not apply to each propellant or every bipropellant combination; the most common problems are [1]:

   - Corrosion: when any propellant gets contaminated with corrosion products, its physical and chemical properties may sufficiently change to make it unsuitable for its intended operation. Corrosion caused by expelled gaseous reaction products is most critical in applications where the reaction products are likely to damage launch or ground test structures and parts of the vehicle.
   - Explosion Hazard: over time some propellants become unstable in their storage tanks and may even detonate under certain conditions, depending on local impurities, temperatures, and shock magnitudes.

- Fire Hazard: many oxidizers will react with a large variety of organic compounds.

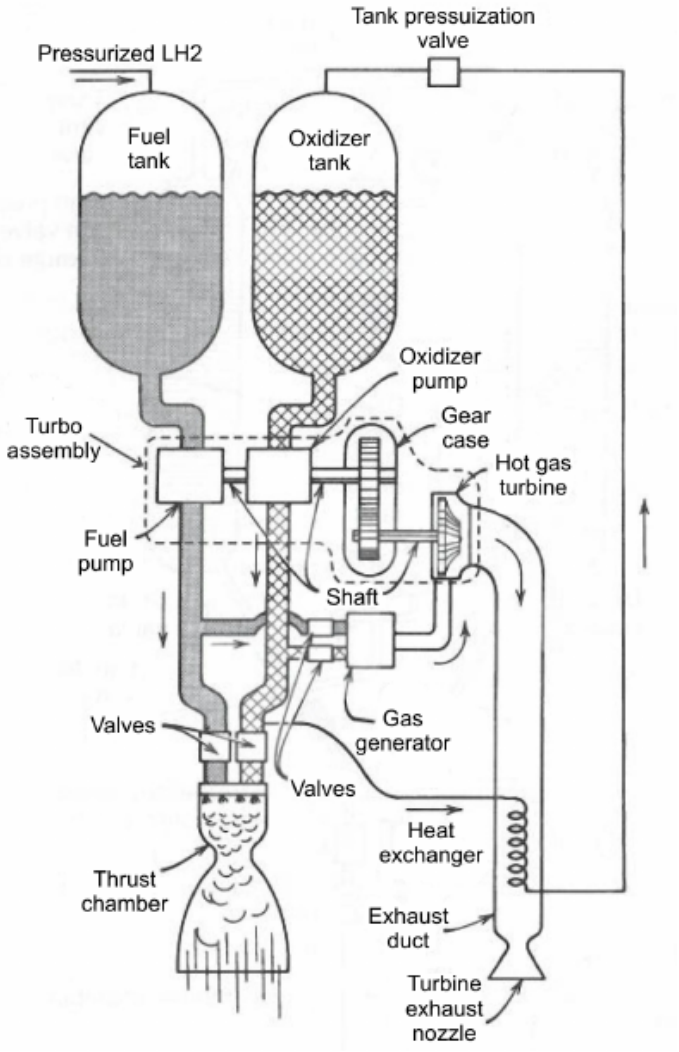


Figure 3: Simple diagram of the liquid propellant engine containing turbopump feed system.

Despite these possible problems related to the storage of propellant, advantages overcome the disadvantages, given the excellent performance that can be achieved with these kinds of rockets.

3. **Hybrid Rocket Engines (HREs)**:
in this last kind of rocket propulsion, oxidant and fuel are stored in different phases. In most cases, fuel is stored in solid form (grain), while oxidant is in the liquid phase. This union is born from the need to solve the LREs' and SRMs' problems. Indeed, SRMs do not allow control while controllability is a main feature of LREs. On the other hand, SRMs are safe and reliable, while LREs are less so because of propellant storage [2].
HREs will be deepened with more details in the following sections because they are the main topic of this thesis work.

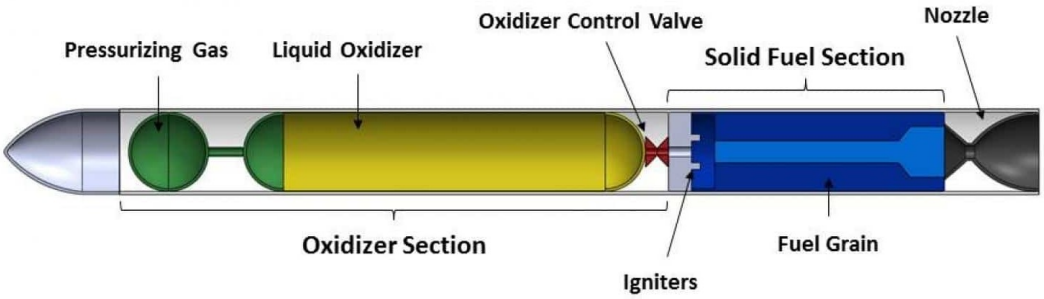


Figure 4: Schematic representation of a HREs.

## 1.3 Hybrid Rocket Engines (HREs)

As mentioned in the previous section, HREs are born to overcome the problems of SRMs and LREs. In particular, the main advantages of hybrid rockets are [1]:

1. More safety and ruggedness than conventional chemical propulsion systems, with less explosion or detonation probability thanks to the propellants' physics separation ;

2. Start, stop and restart capabilities, if the mission requires it;

3. Relative simplicity compared to LREs and, consequently, low overall system cost;

4. Higher specific impulse than SRMs: $I_s^{HREs} > I_s^{SRMs}$;

5. Higher density-specific impulse than many usual liquid bi-propellant engines: $I_\rho^{HREs} > I_\rho^{LREs}$;

6. Continuous regulation capability depending on the required thrust level.

On the other hand, the disadvantages of hybrid systems are [1]:

1. Mixture ratio and consequently specific impulse may vary during the smooth operation, as well as during throttling; this feature of HREs is intrinsic to the functioning of these thrusters. Specifically, during operation, the fuel grain burn and consequently the quantity of fuel produced grows according to the greater surface concerned; this has the consequence, if the oxidant flow is stationary, a drift of the MR from the initial value. This condition is called mixture ratio shifting;

2. Regression rate lower than SRMs one. This results in low thrust density and a high rockets length/diameter ratio ($L/D$);

3. Relatively complicated solid grain geometries are needed, because of the low regression rate, with significant fuel residues. These residues reduce the mass fraction and may vary randomly with the throttling;

4. Density-specific impulse lower than SRMs one: $I_\rho^{HREs} < I_\rho^{SRMs}$;

5. The last point affects the scaling issues. HREs currently in operation are few, and they are designed to equip small rockets. Solving this scalability problem will be fundamental to increasing the number of operational HREs.

Some solutions to these issues will be presented later in this section.

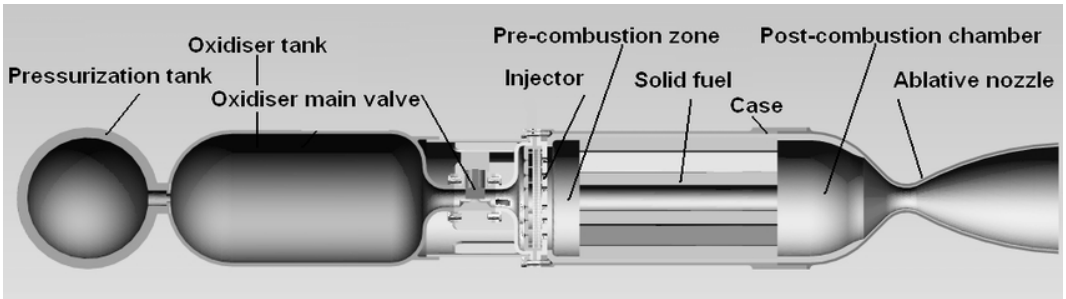


Figure 5: HRE accurate scheme, classical configuration.

Anyway, the most common design for an HRE, called classical configuration, presents liquid oxidant and solid fuel. The oxidizer can be either a storable or a cryogenic liquid depending on the application and the required specific impulse. Usually, this configuration is coupled with a pressurized feed system.

### 1.3.1 Applications and propellants

Thanks to the advantages mentioned in the previous section, hybrid rocket engines are well suited to applications or missions requiring [1]:

- throttling;
- command shutdown and restart;
- long duration missions requiring storable and non-toxic propellants manufacturing and launch operations that benefit from non-self-degradation propulsion systems.

Such applications may include boosters for the primary stage of space launch vehicles, as well as upper-stage and satellite manoeuvring thrusters. In recent years development efforts have concentrated on prototypes for space launch applications, departing from previous military applications.

About propellants, different combinations have been tried over the years; the kind of combination depends on the vehicle [2]:

- For upper-stage missions, which last several months, a combination of Hydrogen peroxide ($HP$) at 90/95%, considerable storable for long periods, and $HTPB$, an poligomer of butadiene terminated at each end with a hydroxyl functional group, used for tire production, is typically used.
- A common propellant combination for large hybrid booster applications has been liquid cryogenic oxygen ($LOX$) with $HTPB$ fuel. The first one is relatively safe and delivers high performance at a relatively low cost.
  Last but not least, this combination produces a non-toxic exhaust gas and is favoured for future booster applications because it is chemically and performance-wise equivalent to the $LOX - RP1$ combination typically of the bipropellant liquid systems.

Now an overview of what are the possible performance improvements concerning modifications made to the Propellants and their combinations is given.
Hybrid propellants may benefit from the addition of powder aluminium to the fuel for some applications. This addition increases the combustion temperature, reduces the stoichiometric mixture ratio, and increases fuel density as well as an overall density-specific impulse (but may reduce the actual specific impulse). On the other hand, hydrogen peroxide ($H_2O_2$) and hydroxyl ammonium nitrate ($HAN$) may result in desirable thermochemical properties, non-toxic exhausts and attractive density-specific impulses [3], [4].
Regarding the ignition system, the case study will be localized in a pre-combustion chamber. This system is necessary to produce the heat necessary for the start of combustion and the following ignition of the whole grain. HRE ignition could be done through hypergolic fluids, solid fuels that ignite spontaneously at ambient pressure and temperature when hit by the oxidant, or through an electrical feed system or, again, with auxiliary gas burners for very small rockets [1].

### 1.3.2 Performance analysis and interior HREs ballistics

The hybrid combustion process, underlying the operation of an HREs, follows the following steps, based on a simplified model for a non-metallized (or low radiation) fuel system [2]:

1. The solid fuel is vaporized thanks to the heat that came from the active combustion zone present in the boundary layer of the mass flow that passes through the grain ports;

2. The vaporized fuel is conveyed to the flame area thanks to the convective motions;

3. Oxidizer convects from the free stream (core flow) to the flame zone by turbulent diffusion. In this zone, the oxidizer meet the vaporized fuel;

4. The combustion process happens inside the boundary layer, where the stoichiometric condition is reached.

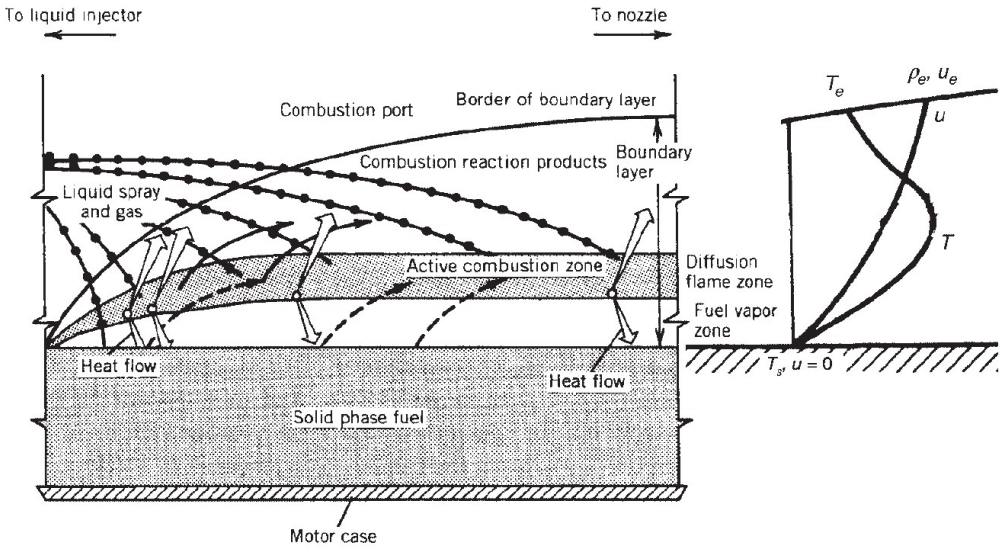


Figure 6: Simplified model of a diffusion-controlled HREs combustion process. $T$ is the temperature and $u$ is the velocity, while the subscript $e$ denotes the zone external to the boundary layer.

This model assumes the previous existence of a fuel and oxidant mass flow that came from the pre-combustion chamber upstream of the solid grain.
Factors beyond pressure and gas temperature affecting the development of the fuel-grain boundary layer, and hence fuel regression characteristics, include grain composition, combustion port oxidizer mass flow rate, and combustion port length and cross-sectional area [1].
Heat transfer relationships between the gas and the solid phase strongly depend on whether the boundary layer is laminar or turbulent. The following figure summarizes the overall behaviour of many oxidizer/solid-fuel combinations. There are three distinct regimes as a function of increasing mass–flow–velocity in the free stream[1]:

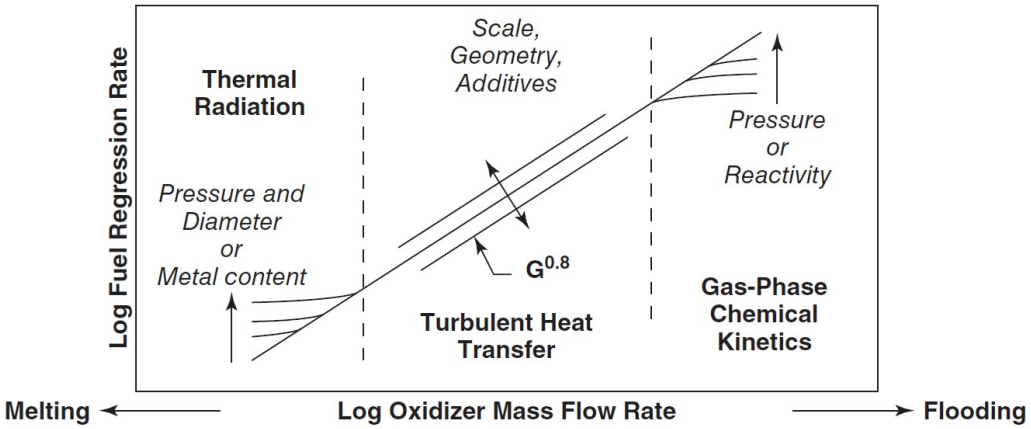


Figure 7: HREs regimes of regression rate dependencies.

1. At the low mass flux regime, radiative heat transfer phenomena are manifest in the form of pressure and diameter effects on the optical transmissivity of the propellant gas, effects which may also arise from any metal loading present; at the "melting limit" or cooking limit the fuel grain may melt, char, or undergo subsurface decomposition.

2. The intermediate region represents fully turbulent heat and mass transfer, and the regression rate dependence on $G^{0.8}$.

3. In the last zone, there are a high value of G and the heat exchanges are led by chemical kinetics; consequently, the regression rate return to be a function of the chamber of combustion pressure. In this region, there is a superior limit for G, caused by a phenomenon named flooding that causes the extinction of the flame.

$G$ is definable as $G = \rho v$ and its value relative to the propulsion field, for fuels unless metals additive, falls in the medium range. For this reason, the thermal radiation is negligible and is possible to consider only convective heat exchanges.
Therefore it is possible to derive an expression for the regression rate, starting from the energy balance exchange through convention inside the turbulent boundary layer [1]:

$$\dot{r} = 0.036 \frac{G^{0.8}}{\rho_f} \left(\frac{\mu}{x}\right)^{0.2} \beta^{0.23} \tag{12}$$

where $G$ is the total oxidant and fuel mass flow per unit area that go through the grain port to a specific axial position $x$, $\rho_f$ is the solid fuel density, $\mu$ is the viscosity of the gases in fuel and $\beta$ is the adimensional mass flow generated from the fuel gasification, evaluate at the surface of the latter;$\beta$ is called the blowing coefficient and can be shown to also represent a nondimensional enthalpy difference between the fuel surface and flame zone.
The equation above indicates that hybrid fuel regression rates in this nonradiative regime are strongly dependent on $G$ and rather weakly dependent on both axial location ($x$) and fuel-blowing characteristics ($\beta$).
It should also be noted that these regression rates are not explicitly dependent on chamber pressure; this is partially true and depends on the propellant.
As propellants move down the combustion port, the gasified fuel being added in the port passage increases the total mass flux. In locations operating at low mixture ratios, this fuel mass increase may be of the same order as the oxidizer mass flow initially entering the port. Given the weak dependence of regression rate on $x$, it would be expected that fuel regression would increase along the flow direction with increases of $G$.
However, it has been observed experimentally that the relationship between the regression rate and the grain length is strongly influenced by other factors like the method of oxidizer injection and by existing precombustion/ vaporization chamber design characteristics.
So, it is not possible to say what kind of trend this quantity follows. Some general trends observed with increasing $x$ are: total mass flux increases, boundary layer thickness growths, flame-standoff distance from the surface increases, combustion port average gas density increases and oxidizer concentration

decreases.
Since the blowing coefficient $\beta$ is not only an aerodynamic parameter but also a thermochemical parameter, and since its $x$ dependence is of the same order, the previous equation is often simplified for purposes of preliminary engineering design by lumping the effects of $x, \beta$, fuel density, and gas viscosity into one parameter, usually given the symbol $a$.
Moreover, in practice, some deviations from the theoretical 0.8-power of the mass velocity exponent are often noted, and for this reason, the semiempirical exponent is indicated with $n$.The resulting simplified form is therefore written as [2]:

$$\dot{r} = a(G_0)^n \tag{13}$$

where $G_0$is the oxidizer mass velocity, i.e. the oxidizer mass flow rate divided by the combustion port cross-sectional area, while the parameters $a$ and $n$ are empirically fitted constants.$\dot{r}$ for an HREs have been observed to have values of the order of a few millimetres per second.
An alternative form of equation (12), to account for an observed pressure and/or port diameter dependency, is written as [1]:

$$\dot{r} = aG_0^n p_c^m D_p^l \tag{14}$$

where $m$ has been observed to vary between $0 \div 0.25$ and $l$ between $0 \div 0.7$.
This equation, show one of the main problems of this kind of rocket, which is the possibility of scaling ballistic performance. The lack of sufficient valid data for different motor sizes has not yet made it possible to better understand the effects of scale.
Nevertheless, computational fluid dynamic (CFD) approaches, that resolve the hybrid flow field appear to offer the best hope for analytically evaluating scale effects.

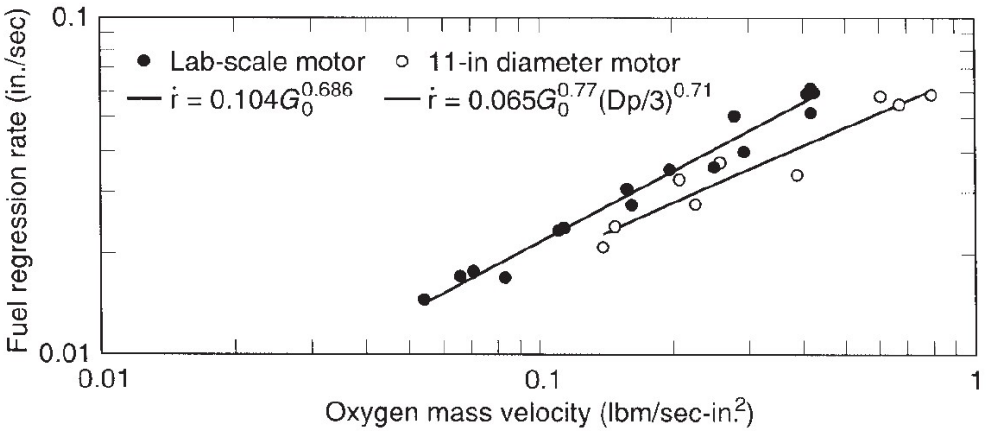


Figure 8: Regression rate decrease with HRE scale, i.e. combustion port diameter, increases.

**The dynamic behaviour analysis in stationary conditions:** Dynamic behavior of an HREs is really complicated to analyze without the aid of simplifying assumptions, but at the same time, it is of particular interest because the mixture ratio always varies even during steady-state oxidizer flow. To analyze this behaviour, the continuity equation is used [1]

$$\frac{\partial(p_c V_c)}{\partial t} = \dot{m}_{in} - \dot{m}_{out} \tag{15}$$

where the quantities associated with the combustion chamber are indicated with c. If stationary conditions are assumed, it can be written [1]

$$\dot{m} = \dot{m}_O + \dot{m}_f = \frac{\rho_c A_t}{c^*} \tag{16}$$

The steady thrust of a hybrid rocket motor can be expressed as [1]

$$F = \dot{m} I_s g_0 = (\dot{m}_O + \dot{m}_f) I_s g_0 \tag{17}$$

Therefore, the HREs regulations can be done by changing the oxidizer flow rate, usually through a throttling valve in the oxide feed line.
Thanks to the previous equation, is easy to notice that the fuel flow is a function of the oxidizer flow, but not necessarily in a linear way. For circular port geometries with inner radius R, the regression rate can be written as [1]

$$\dot{r} = a\left(\frac{\dot{m}_o}{\pi R^2}\right) \tag{18}$$

accordingly to [1], the mass flow rate of fuel is given by

$$\dot{m}_f = \rho_f A_b \dot{r} = 2\pi\rho_f R L \dot{r} \tag{19}$$

where$A_b$ is the combustion port surface area and $L$ is the port length. Combining eq (18) and (19), the fuel production rate is obtained in terms of port radius and oxidizer mass flow rate [1]

$$\dot{m}_f = 2\pi^{1-n}\rho_f L a \dot{m}_o^n R^{1-2n} \tag{20}$$

Thanks to this equation, is possible to see the dependency between oxidizer flow and fuel flow, which is non-linear.
A separate case is that in which $n = 0.5$ and therefore $\dot{m}_f \propto \dot{m}^{0.5}$ and the fuel flow is independent of the size of the grain openings. In this case, by reducing the oxidizer flow by half, there will be a reduction in the fuel flow rate of 0.707 and consequently, the thrust will change in a non-linear way, as previously mentioned.
Usually, as thrust is decreased by reducing oxidizer flow, the mixture ratio ($\dot{m}_O/\dot{m}_f$) is also reduced, becoming increasingly fuel rich. In some HRE concepts, a portion of the oxidizer is injected into a mixing chamber downstream of the fuel grain, to maintain a more constant $MR$.
Equation (20) also indicates that, for constant oxidizer flow, fuel flow will increase with increasing port radius if $n < 1/2$. For $n > 1/2$ (i.e. majority of cases), fuel flow will decrease with increasing port radius.

### 1.3.3 Solutions for improving the regression rate

Some solutions to improve the low regression rate of HREs are :

- A multi-port grain geometry for the solid fuel: considering fixed combustion surface $A_b$ and passage surface $A_p$, the grain length can be reduced by increasing the combustion perimeter and, so, decreasing the length to diameter ratio ($L/D$) of the Rocket.
- $MR$ high values: increasing the MR, the contribution of fuel flow decreases (vice-versa for the oxidizer flow rate), causing a decrease in the regression rate. The benefits of this approach are connected with the choice of propellants with high values of c, for high MR values.

These two solutions are applicable to mitigate particular negative effects that arise due to low values of the regression rate.

- Addition of energetic particles: addition of metal particles in the polymer-based solid fuel, involves the increase of $I_s$ and $I_\rho$ and consequently increases the regression rate, at the expense of some multiphase flow losses. The main metals used in the current research are aluminium, lithium and boron, because their chemical characteristics, like easy ignition, high reactivity and high calorific value, are favourable for use inside grain of fuel [5].
- Use of energy polymers: the replacement of the usually inert binder, used for grains in HREs, with a polymer or a plasticizer with a high energy content increases the amount of total energy of the fuel/oxidizer combination used and, consequently, the regression rate. The main disadvantage is the safety of the rocket [4].
- Use of paraffin-based and cryogenic fuels: the regression rate of paraffin-based fuels is about 3/4 times greater than that of conventional fuels. This fact is due to the generation of a thin liquid layer on the surface of the grain, from which they come ejected fuel droplets towards the boundary layer. The flow of mass of fuel that is obtained is not driven by the mechanisms of heat exchange between gases and is not limited at the top by blocking phenomena [4].

The three approaches just discussed are applicable to improve the regression rate.

- Use of non-conventional geometry for solid fuel grain: in this case, the aim is to improve performance by modifying the structure of the flow of the solid grain. The consequence is the generation of three-dimensional flows of recirculation and the boundary layers separation.
- Use of vortex injectors: this solution guarantees the reduction of both grain thin and the boundary layer.

These last measures aim at increasing the thermal flux between the flame zone and the surface of the solid grain. The latter is responsible for the gasification of the fuel and therefore determines the regression rates [5].

# 2 Engine Optimization

## 2.1 Engine Design and Optimization

As mentioned in the previous sections, a three-stage launcher for small satellites is considered, with six, three and one engine for each stage (first, second and third stage, respectively) [7].
The hybrid motor employs liquid cryogenic oxygen (LOX) as an oxidizer and a solid paraffine-based as a fuel. This propellant combination presents a good specific impulse and a large regression rate. The promising performances for which this type of rocket turns out to be interesting come to light for applications such as sounding rockets and upper stages.
A chamber pressure $p_c = 10bar$ is assumed, while the maximum internal pressure of the tank is considered equal to $25bar$. This last pressure will be modified in a preliminary phase taking into account the contribution of the fluid column, calculated through Stevino's law, which allows calculating the additional part of pressure given by the gravity acceleration and the fluid density, as the altitude at which the body is located varies, in the following way:

$$P_{column} = \rho_{column}\left(l_{tank}\right) = 9.81\left(\rho_{ox} G_{t_{max}}\right) l_{tank} \tag{21}$$

where $g = 9.81$ is the value of the acceleration of gravity on the earth's surface, $\rho_{ox}$ is the density of the oxidant, $G_{t_{max}}$is the maximum longitudinal load factor, assumed equal to 6.5, and $l_{tank}$ is the tank length, that defines the altitude of fluid into the body.
Thanks to this law, the tank's internal pressure become:

$$P_{tank} = P_{tank_i} + P_{column} \tag{22}$$

The contribution of the fluid olumn $P_{column}$ is taken into account in the preliminary evaluation of the structural integrity of the tank but is neglected in HRE performance evaluation. In fact, this value of pressure shall be greater than the critical pressure of the external loads, in order to not compromise the structural integrity of the launcher tank/s.
Even though the actual pressure in the combustion chamber can span over a wide range during motor operations, the error is small for chamber pressures and mixture ratios considered in this thesis work. An ideal frozen equilibrium of the gas composition is assumed to evaluate $c^*$, which will be corrected later through a constant even to 0.96. The thrust coefficient is evaluated as a function of the nozzle area so that the expansion ratio and the ambient pressure are defined. A factor of 0.98 is introduced to take losses into account and to reduce the thrust coefficient value.
A cylindrical grain with a single circular port is considered and a uniform regression rate along the port axis is assumed. Under these hypotheses, it can be re-written [6], [7]

$$\dot{r} = \frac{dR}{dt} = a\left(\frac{\dot{m}_o}{A_p}\right)^n \propto \dot{m}_o R^{-2n} \tag{23}$$

with $a = 9.1 \bullet 10^{-5} m^{2n+1} s^{n-1} kg^{-n}$ and $n = 0.69$ [7]. The International System of Units (SI) is used.
No pyrolysis of the lateral ends is considered. The chamber head-end pressure $p_{c1}$ depends on the chamber/nozzle stagnation pressure $p_c$ according to an approximate relation similar to that proposed by Barrere [20] for side-burning grains [7]

$$p_{c1} = \left[1 + 0.2\left(\frac{A_{th}}{A_p}\right)^2\right] p_c \tag{24}$$

The oxidizer flow rate is determined through the hydraulic resistance $Z$ in the oxidizer flow path from the tank to the combustion chamber; this parameter is assumed to be constant during motor operation. Another hypothesis is to consider an incompressible turbulent motion regime for the flow and, consequently, the oxidizer flow is [7]

$$\dot{m}_o = \sqrt{\frac{(p_t - p_{c1})}{Z}} \tag{25}$$

The fuel mass flow is [7]

$$\dot{m}_f = \rho_f A_b \frac{dR}{dt} \propto \dot{m}_o^n R^{1-2n} \tag{26}$$

These two mass flows allow the calculation of the mixture ratio [7]

$$\alpha = \frac{\dot{m}_o}{\dot{m}_f} \propto \dot{m}_o^{1-n} \bullet R^{2n-1} \tag{27}$$

Under the assumption of an isentropic expansion, the chamber pressure can be written in the following way

$$p_c = \frac{(\dot{m}_o + \dot{m}_f)\, c^*}{A_{th}} \tag{28}$$

A simple blowdown system is chosen to maintain a low level of complexity [7]. The pressurizing gas Helium is adopted.
The liquid oxidizer in the tank, thanks to this system, is going to be pressurized by the residual gas "ullage", in our case helium precisely. This ullage is compressible and expandable. Otherwise, the liquid propellant is incompressible, so it relies on gas pressure above the liquid level to push down on the liquid and push it through the drain at high speeds and pressures [6]. Because the gas is compressible, it will expand to take up the space that was previously occupied by the liquid oxidizer but at the cost of some of its pressure.
According to the chosen ballistic model, the design of this hybrid rocket engine is defined by the initial thrust ($F_i$), the initial mixture ratio ($\alpha_i$), the expansion ratio of the nozzle ($\varepsilon$), tank pressure value ($P_{t_i}$) and the initial filling volume ($V_{g_i}$) [7]. Two of these parameters, i.e. the thrust and the expansion ratio of the nozzle, are fixed, while the others are left free in order to be optimized by the direct method. Also, an initial value of the chamber pressure is fixed at $P_{c_i} = P_{t_i}/2.5$ in order to avoid coupling between the hybrid engine and the oxidizer feed system during normal rocket operations.
Finally, the initial port area ratio ($J$) value is fixed at 0.5 in order to avoid excessive pressure losses and a regression rate non-uniform, but theoretically should be as large as possible at the expense of tank pressure, which tends to be very low when this parameter is left free.
Given this set of input parameters, the motor geometry is first determined. From $\alpha_i$ is possible to obtain the initial value of $c^*$ and $\gamma$. Thanks to $\varepsilon$ the pressure ratio $p_e/p_c$ is calculated. Also, the thrust coefficient $C_F$ and $c = c^* \bullet C_F$ can then be evaluated, if the ambient pressure is known. The initial thrust $F_i$ gives the mass flow rates at ignition [7]

$$(m_P)_i = (1+\alpha_i)(\dot{m}_f)_i = \frac{1+\alpha_i}{\alpha_i}(\dot{m}_O)_i = \frac{F_i}{c_i^*(C_F)_i} \tag{29}$$

Inverting Eq. (26), the throat area could be determined; in this analysis, the phenomenon of throat erosion is neglected. The initial port area and radius are obtained as

$$(A_p)_i = \pi R_i^2 = \frac{A_{th}}{J} \tag{30}$$

Also, the initial burning area ($A_b$) is determined from Eq. (24), and the grain length is consequently calculated as

$$l_g = \frac{(A_b)_t}{2\pi R_t} \tag{31}$$

thus defining the initial grain geometry. Finally, the tank pressure, which rules engine operation, during blowdown is calculated assuming an isentropic expansion of the pressurizing gas in the tank

$$p_t = (p_t)_i \left[\frac{(V_g)_i}{V_g}\right]^{\gamma_g} \tag{32}$$

where $V_g$ is the gas volume in the propellant tank (gas “ullage”) at time t, calculated like $V_g = (V_g)_i + m_O/\rho_O$.
This ullage is compressible and subsequently expandable. The liquid propellants are incompressible, so it relies on gas pressure above the liquid level to push down on the liquids and push them through the drain at high speeds and pressures. Because the gas is compressible, it will expand (previous hypothesis) to take up the space that was previously occupied by the liquids but at the cost of some of its pressure.
There are different approaches to solving engine optimization. Using the Deterministic Approach Eq. (21-30) are numerically solved to evaluate the regression rate, the propellant flow rates (and their ratio $\alpha$), the chamber pressure $p_c$ and $p_1$, while the curve fit $c^*$ as a function of $\alpha$ is used. After this, the thrust level is determined through the following equation [6], [7]

$$F = p_c A_{th} C_F \tag{33}$$

where the thrust coefficient ($C_F$) is evaluated at the actual altitude, in order to integrate the trajectory equations. At burnout, the web thickness w and the grain outer radius $R_f = R_i + w$ are obtained; the

overall propellant mass and an estimation of the structural masses are taken into account to compute the engine's overall mass.
The dry mass of the propulsion system is made of a combustion chamber, nozzle, tanks and rocket casing. All these quantities are estimated through suitable assumptions and approximations. The combustion chamber has an insulation liner (with the same density as the solid fuel) and a cylindrical wall. The diameter of the oxidizer tank is selected in order to have a given overall finesses ratio (length to diameter ratio) [7]. The wall thicknesses of the oxidizer tank, gas tank, and combustion chamber are determined to withstand internal pressure, assuming some safety factors. Each HRE is encapsulated by a cylindrical casing, which thickness will be reported later as it varies with the variation of the material. A 45-deg convergent and a 20-deg divergent nozzle (half-opening angle) with a phenolic silica ablative layer is considered. A uniform thickness is assumed and evaluated to estimate the nozzle weight. The adopted thickness is half the value obtained according to Reference [7] for the throat thickness; average values of the transport properties and an estimation of the heat flux at ignition are used. The nozzle structural mass is small compared to this ablative layer mass and is thus neglected. In this way, the engine design parameters are optimized.
Tentative values are initially assumed for the free design parameters, mentioned above, and then the ascent trajectory is optimized using an indirect procedure to evaluate the payload, as described in the following section. Perturbation of the design parameter allows one to numerically evaluate the derivatives of the performance index and a procedure based on Newton's method is used to determine the set of design parameters which simultaneously nullify the index partial derivatives. Only a few minutes are sufficient to obtain the optimal design and the corresponding trajectory.

## 2.2 Trajectory Optimization

The following chapter concerns the trajectory optimization method based on what is presented by L. Casalino, F. Masseni, D.Pastrone in their work "Hybrid Rocket Engines for Small Satellite Launchers" [7]. An airborne launch is considered with starting conditions similar to the Pegasus launcher (the rocket is brought up to a certain altitude by an carrier aircraft and then released in flight to be able to ignite the stages and reach the design orbit).


Figure 9: Pegasus rocket ready for airborne launch with NASA scientific satellite.

Rocket ignition occurs at $12\,km$ altitude, $45 - deg$ latitude and $250\,m/s$ relative speed, following a pull-up maneuvre which is not modelled in this analysis. Payload is delivered to a reference circular orbit with $95 - deg$ inclination (launch from 45 degrees latitude) and altitude equal to $800\,km$. Also, the direction of the initial velocity is assumed to be left free. The free molecular heat flux, calculated

as $\Phi = \frac{1}{2}\rho V_{rel}^3$, must remain below $0.1 BTU/ft^2/s$ after fairing jettisoning (which occurs at second stage burnout). This is achieved by forcing a steep ascent trajectory with the introduction of a height constraint at the end of the third stage first burn, which occurs at 160 km; this limit value is obtained as follows: $h_{constraint} = (r_{lim} - 1) \bullet R_{conv}$, where $r_{lim} = 1.025\,Km$ and $R_{conv} = 6378\,Km$ (this second parameter is the hearth radius) [7].
During the first-stage burn, the vehicle follows a zero-lift gravity-turn trajectory with thrust parallel to the relative velocity. The thrust direction is left free and optimized for the second and third stage burns. The third stage performs two burns with the second one that is very short for the orbit circularization. The ascent trajectory is therefore modelled with the following phases [7]:

1. Zero-lift gravity-turn first-stage burn;
2. 8-second coast arc for stage jettisoning;
3. Second stage burn considering the optimal thrust direction;
4. 8-second coast arc for stage and fairing jettisoning;
5. Also, an optimal thrust direction is assumed for the first combustion of the third stage;
6. Coast arc (free length);
7. Finally, Third-stage second burn with optimal thrust direction for circularization.

The $j$-th phase starts at time $t_{f-1}$ and ends at $t_j$. A deterministic approach is used to maximize the final mass of the rocket.

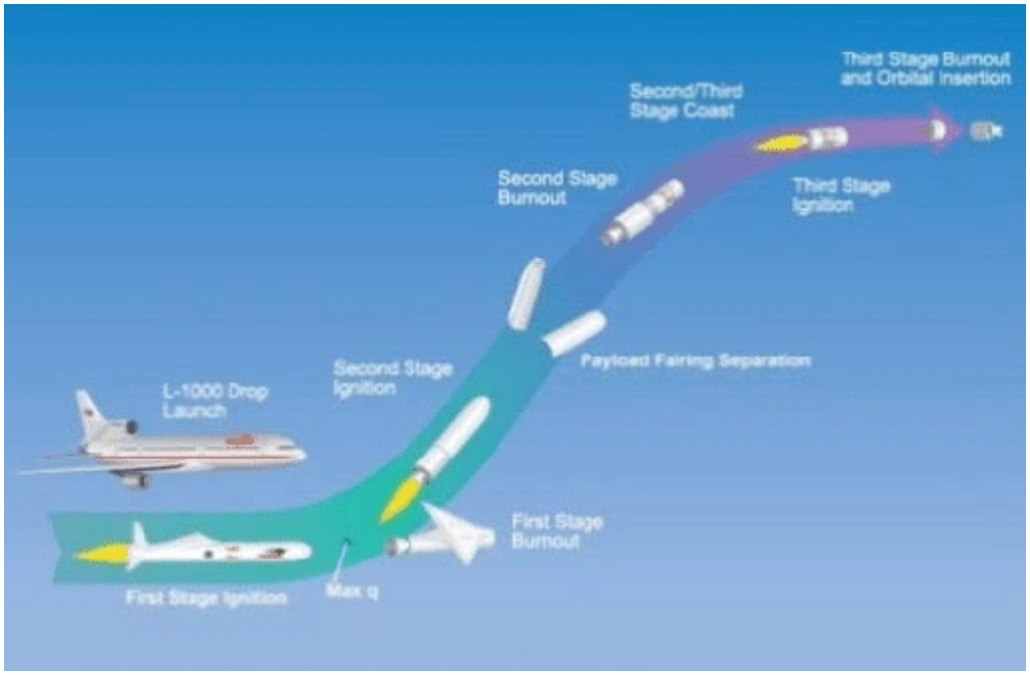


Figure 10: Stages of the Pegasus launch and separation system.

In the continuation of the discussion, the rocket is considered as if it were a point mass and, consequently, the equations of state in an inertial reference system centred on the Earth, in a dimensionless form, in this case, are

$$\frac{d\boldsymbol{r}}{dt} = \boldsymbol{v} \quad \frac{d\boldsymbol{v}}{dt} = -\frac{\boldsymbol{r}}{|\bar{\boldsymbol{r}}|^3} + \frac{\boldsymbol{F} - \boldsymbol{D}}{m} \quad \frac{dm}{dt} = -\frac{F}{c} \tag{34}$$

where an inverse-square gravity field has been assumed and $D = (1/2)\rho_{atm} C_D S v_{rel}^2$ is the aerodynamic drag. The reference area in the above formula is the sum of the cross sections of the HRE used in each ascent phase, and is therefore determined by the design of the HRE itself. The relative velocity is $\boldsymbol{v_{rel}} = \boldsymbol{v} - \boldsymbol{\omega} \times \boldsymbol{r}$ where $\omega$ is Earth's angular velocity.

The drag coefficient $C_D$ is assumed to vary with the Mach number according to a typical law for Rockets, as is possible to see in Fig.11, to take the most relevant effects of its influence into account; the same law is used for all the stages. This function trend is the same as the Reference [7], the paper relative to this case of study.

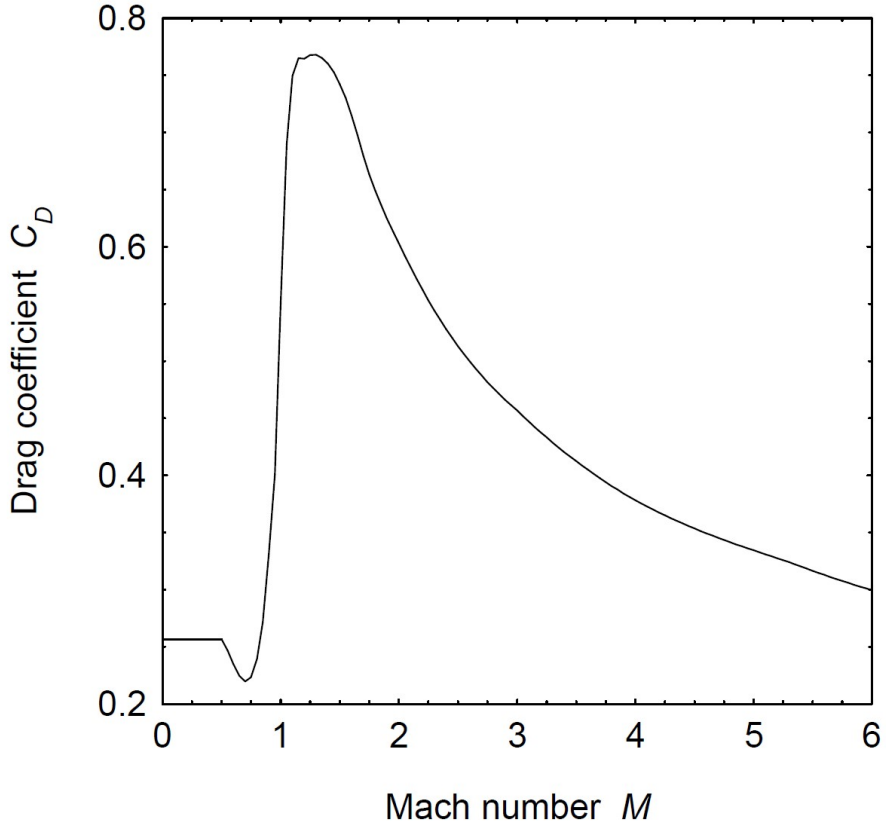


Figure 11: The Drag coefficient $C_D$ in function on the Mach number $M$ [7].

The thrust is written as a function of the vacuum thrust

$$F = F_{vac} - EA_{th}p_{atm} \tag{35}$$

where $F_{vac}$ is a given function of time once the engine design has been specified [7].
Numerical fits of Earth's atmosphere are used in order to determine, as functions of the altitude $h$, the pressure and the temperature, according to a simplified model. Some boundary conditions are necessary, such as the fixing of the initial position (at $t_0 = 0s$), of the relative velocity and of the mass. At the final time $t_f$, insertion into a circular orbit with a specified inclination is imposed (radius, vertical velocity, horizontal velocity and inclination are fixed) in the deterministic approach.
Therefore, two additional conditions are introduced, i.e. $t_1 = t_3 - t_2 = t_7 - t_6 + t_5 - t_4$ . Also, the coast arcs $t_2 - t_1 = t_4 - t_3$ are given. As already stated, the height at $t_5$ is fixed in the deterministic approach.
The theory of optimal control is applied to optimize the trajectory, once the characteristics of the stages are assigned. Adjoint variables are associated with the state equations and the Hamiltonian, which has different expressions depending on the phase of flight, is defined [7]

$$H = \boldsymbol{\lambda}_r \boldsymbol{v} + \boldsymbol{\lambda}_v \left( \frac{\boldsymbol{r}}{|\bar{\boldsymbol{r}}|^3} + \frac{\boldsymbol{F} - \boldsymbol{D}}{m} \right) - \lambda_m \frac{F}{c} \tag{36}$$

Optimal control theory provides the Euler-Lagrange equations for the adjoint variables [7]

$$\frac{d\boldsymbol{\lambda}_r}{dt} = -\frac{dH}{d\boldsymbol{r}} \quad \frac{d\boldsymbol{\lambda}_v}{dt} = -\frac{dH}{d\boldsymbol{v}} \quad \frac{d\lambda_m}{dt} = -\frac{dH}{dm}$$

The optimal control theory (OCT) provides the thrust direction, when it is left free, which results to be parallel to the velocity adjoint vector, also named the primer vector. OCT also provides boundary conditions for optimality at the initial and final point and at the boundaries of each phase [7]. The dual problem of radius maximization for a given HRE mass (that is, payload) is preferred as it allows for an easier derivation of the optimality conditions. We obtain that the velocity vector added, at the initial instant (t=0), must be parallel to the relative velocity vector; to this are added the two additional conditions to the final time (here omitted), which relate the position and velocity values with their added variables. In addition, OCT provides the transversality conditions to determine the relevant times.So, in this formulation, time is formally free (the time boundary conditions become mass constraints) and the Hamiltonian must be continuous at time $t_5$ and $t_6$ and null at $t_7$. At $t_5$ the radius adjoint variable has a free discontinuity and is an additional optimization variable; also,$\lambda_{rf} = 1$ and it is conveniently replaced by $\lambda_{r0} = 1$, reducing the number of unknowns [7]. The added mass variable has free discontinuities between times $t_1$ and $t_4$ so as to ensure the continuity of the Hamiltonian function; these discontinuities can be ignored as $m$ does not appear in the equation for the other variables and boundary conditions at those points. The problem of the multipoint boundary value, which arises from the application of the theory of optimal control, is solved by means of a procedure based on Newton's iterative method.

Tentative values are initially chosen for the problem unknowns and progressively modified to fulfil the boundary conditions.

# 3 Mass Budgeting

This section presents an overview of the mass budgeting of the rocket, with a particular focus on the mathematical model of the FORTRAN code, used to optimize the payload mass, once the best material-geometry pair has been identified.
The analysis of the FORTRAN code will be divided into the following phases:

1. Overview of the reference case: description of the model and the definition of the input values;

2. Summary of the cases implemented, i.e. hypotheses relating to the geometries, the definition and assumption regarding the latter, etc.

## 3.1 Reference test case

In the Reference study case, the following input values are considered [7]:

| Quantities | Symbols | Input value |
|---|---|---|
| Initial tank pressure $[bar]$ | $P_{t_i}$ | 25 |
| Nozzle expansion ratio | $\varepsilon$ | 14 |
| Ullage Volume $[m^3]$ | $V_{g_i}$ | 0.253 |
| Initial Trust $[kN]$ | $F_i$ | 11.5 |
| Initial Mixture ratio | $\alpha_i$ | 1.86 |

Table 1: Input of the reference case study.

Also, the combustion chamber pressure was previously defined, as the predefine orbit that the launcher shall reach, and the interstage and fairing masses, are the fixed part of the initial mass of the Rocket.
In the reference case [7], a cylindrical tank with spherical shells made of aluminium alloy was considered. The calculation of the radius of the tank started from the calculation of the internal and external radius of the grain. This last value was added to the thickness of the liner in order to obtain the radius of the combustion chamber.
Finally, it was assumed that the tank radius was at first equal to that of the combustion chamber. Subsequently, the true value of the radius of the tank is obtained through an iterative method: this process consists to find a value of the tank radius which satisfy the condition according to which the ratio length/diameter $(L/D)$ of the rocket must be equal to 10. In addition to the iterative just mentioned, numerous other quantities are calculated for the project. The initial mass of the launcher is given and is equal to 5000 kg. Of these, there is a fixed part given by two contributions, i.e. the interstage 1-2 adapter mass equal to 50 kg and the interstage 2-3 adapter, plus fairing (jettisoned at stage 2) equal to 35 kg. As for the calculation of the other principal masses, this is presented here.:

- Propellant mass: is the mass of propellant consumed during the mission by each engine, and is the sum of the mass of fuel and mass of oxidizer consumed. It is calculated as follows

$$m_{prop} = \frac{m_{rocket}\,(1 - f_{prop})}{n_{engine}} \tag{37}$$

where, $m_{rocket}$ is the initial mass of the launcher, defined above, $f_{prop}$ is the propellant fraction consumed in each phase of the mission and $n_{engine}$ is the number of engine, respectively six for the first stage, three for the second one, and one for the last. Instead, the mass of fuel is calculated based on the fact that the grain is a hollow cylinder [7]. Consequentially

$$m_{fuel} = \pi \left( r_{g_f}^2 - r_{g_i}^2 \right) l_{grain} \rho_{fuel} \tag{38}$$

where, $r_{g_f}$ and $r_{g_i}$ are the external and internal radius of the drilled grain, $l_{grain}$ is the grain length, and $\rho_{fuel}$is the fuel density.
Thanks to these two equations it is possible to obtain the mass of oxidant, as

$$m_{ox} = m_{prop} - m_{fuel} \tag{39}$$

- Pressurizing gas mass: the choice of a blowdown supply system implies that the calculation of the mass of pressurized gas can be performed by inverting the law of perfect gases which, with a fixed ullage volume and a fixed pressure, can be written in the following way

$$m_{gas} = p_{t_i} \frac{v_{g_i}}{R_{gas} T_{gas}} \tag{40}$$

  where $p_{t_i}$is the initial tank pressure, $v_{g_i}$ the ullage volume and both are defined in the previous chapter, whereas $R_{gas}$ and $T_{gas}$ are the universal gas constant and gas temperature, both referred to the pressurizing gas chosen, the Helium.

- Total mass of the tank: for the calculation of the tank mass the following equation was used

$$m_{tank} = 2\rho_{tank}\pi r_{tank} l_{tank} s_{tank} \tag{41}$$

  where $\rho_{tank}$ is the tank material density (in this case equal to the alluminum density), $r_{tank}$ is the tank radius obtained through the iterative process explained above, $l_{tank}$ obtained from the sum of the cylindrical length and the contribution of the spherical shells ($l_{tank} = l_{cyl} + 2r_{tank}$), and $s_{tank}$ that is the thickness of the tank.

- Dry masses: those quantities included the masses of the following structural components: case, combustion chamber, nozzle, pressurizing gas and tank. Each dry mass is calculated by adding these components and multiplying this mass by the number of engines in the reference stage

$$m_{dry} = (m_{case} + m_{tank} + m_{gas} + m_{cc} + m_{nozzle}) n_{engine} \tag{42}$$

- Payload mass: this mass is particularly important because, with the same initial weight, the higher it is, the greater the payload that can be inserted into orbit with a single launch. This has an economic advantage. The value of the Payload mass is obtained starting from the initial mass of the rocket from which the mass of propellant, the mass of the previously mentioned fixed components and the dry masses are subtracted. This results in the following equation:

$$m_{payload} = m_i - m_{1-2} - m_{2-3\&fairing} - m_{dry1} - m_{dry2} - m_{dry3} - (m_{prop} \bullet n_{engines}) \tag{43}$$

  where $n_{engines}$ is the number of all engine, equal to 10, while the other masses are defined above. Therefore, as can be seen from the formula, the lower the dry masses of the stages will be and, with the same initial weight, the greater the obtainable payload.

- Final mass: this last mass is $m_F = m_{dry3} + m_{payload}$ and indicate the final mass after the separation of both first and second stages, but before the separation of the payload mass from the launcher.

Also, the equation used for the calculation of the other quantities are shown:

- Tank radius and Rocket's diameter: the iterative procedure used to calculate the radius of the tank has been explained above. To this radius, the thicknesses of the case and the tank are added

$$r_{rocket} = r_{tank} + s_{case} + s_{tank} \tag{44}$$

$$D_{rocket} = 2 \bullet r_{rocket} \tag{45}$$

- By doing so, a very important size is obtained, i.e. the diameter of the launcher: this size is of such importance because the ratio of the rocket length to diameter is given, and the iterative process just mentioned is based on this size. In fact, in input, an $(L/D)_{rocket}$ value, also called Aspect ratio, equal to 10 is imposed, and the iterative calculates the best L and D values with which to obtain the value of this ratio. Lower $D_{rocket}$ values lead to improved performance. In fact, Rockets with a larger diameter have more drag because there is more air being pushed out of the way. Drag depends on the cross-sectional area of the object pushing through the air

$$D = \frac{1}{2}\rho v^2 C_D A \tag{46}$$

  Making a rocket as narrow as possible is the best way to reduce drag.

- Rocket's length: this is the second geometric quantities that is particularly important for design purposes. As mentioned for the diameter of the rocket, its length is also necessary to calculate the Aspect ratio. It is obtained through the evaluation of the following contributions

$$L_{rocket} = l_{grain} + l_{tank} + l_{nozzle} \tag{47}$$

where $l_{grain}$ and $l_{tank}$ are defined above, while $l_{nozzle}$ is calculated through the hypothesis of a convergent-divergent nozzle with a convergent opening angle of 45° and a diverging opening angle of 20°.

- Tank Volume: obtained through the following equation

$$V_{tank} = \frac{m_{ox}}{\rho_{ox}} + v_{g_i} \tag{48}$$

in which the quantities present have been previously mentioned, is of particular interest as it allows us to calculate the length of the cylindrical portion of the tank and consequently the length of the rocket. This, starts from a simple equation, based on an evaluation of the volume necessary to contain the oxidant mass, to which is added the volume part relating to the pressurizing gas.

- Thicknesses of the components: evaluating the thickness of the components, the following formula, deriving from the shell theory [12], was used

$$s_{component} = P_{ref} \frac{r_{ref}}{\sigma_{material}} \tag{49}$$

where $P_{ref}$ and $r_{ref}$ are respectively the pressure and the radius of the reference components, i.e. the tank rather than the combustion chamber, etc. Instead, $\sigma_{material}$ is the ultimate tensile strength divided by a safety coefficient, equal to 1.25 [11].

In this case, the values obtained through the optimization process are shown in the following table:

| | Symbols | Reference case value |
|---|---|---|
| Propellant mass $[kg]$ | $m_{prop}$ | 425.7 |
| Fuel mass $[kg]$ | $m_{fuel}$ | 134.2 |
| Oxidiant mass $[kg]$ | $m_{ox}$ | 291.5 |
| Pressurizing gas mass $[kg]$ | $m_{gas}$ | 1.01 |
| Total mass of the tank $[kg]$ | $m_{tank}$ | 18.92 |
| Combustion chamber mass $[kg]$ | $m_{cc}$ | 11.1 |
| Nozzle mass $[kg]$ | $m_{nozzle}$ | 9.97 |
| Mass of the case $[kg]$ | $m_{case}$ | 20.01 |
| Dry Mass 1 $[kg]$ | $m_{dry1}$ | 365.94 |
| Dry Mass 2 $[kg]$ | $m_{dry2}$ | 182.97 |
| Dry Mass 3 $[kg]$ | $m_{dry3}$ | 61 |
| Tank volume $[m^3]$ | $V_{tank}$ | 0.51 |
| Tank radius $[m]$ | $r_{tank}$ | 0.238 |
| Rocket's diameter $[m]$ | $D_{rocket}$ | 0.48 |
| Thickness of the tank $[mm]$ | $s_{tank}$ | 1.5 |
| Combustion chamber thickness $[mm]$ | $s_{case}$ | 0.5 |
| Tank lenght $[m]$ | $l_{tank}$ | 2.54 |
| Nozzle lenght $[m]$ | $L_{nozzle}$ | 0.64 |
| Rocket's lenght $[m]$ | $L_{rocket}$ | 4.8 |
| Payload mass $[kg]$ | $m_{payload}$ | 48.1 |
| Final mass $[kg]$ | $m_F$ | 109 |

Table 2: Reference case values.

## 3.2 Presentation of the implemented geometries

In the previous subsection the reference case was presented, that is the case of a cylindrical tank with spherical shells, in aluminium alloy. Instead, in this chapter the new geometries used will be presented; unlike the previous chapter geometry, they will not be associated with any material. On the contrary, in the next chapter, all the materials used will be analyzed, and by associating these with the geometries that will now be presented, the results of the optimization process will be shown and analyzed.
In the following sub-chapters, the input data will not be repeated as they remain the same as those presented in the reference case.

### 3.2.1 Cylindrical tank with ellipsoidal shells

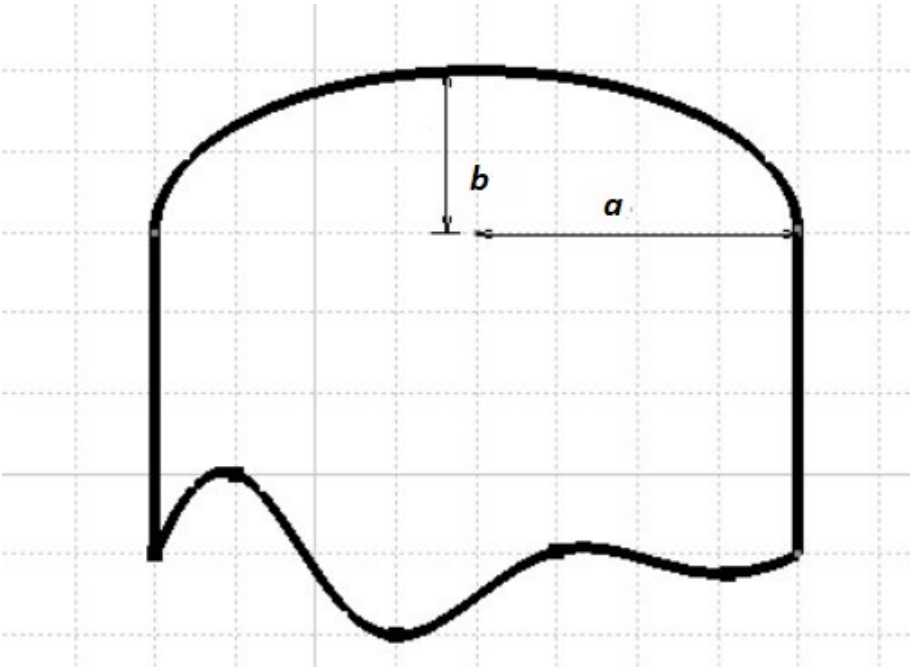


Figure 12: Sketch of the cylindrical tank with ellipsoidal shells.

For the design of this geometry, we started with some assumptions [8]. First of all, the initial radius of the cylindrical tank, i.e. the semi-major axis of the ellipsoidal shells ($a$), was placed equal to the value of the external radius of the grain ($r_{g_f}$). This quantity was subsequently linked to the height of the ellipsoidal shells, that is the minor semi-axis of the ellipsoidal ($b$), through a parameter named Ellipse ratio ($ER$). This is the ratio of its sizes in different dimensions. For a circle, this quantity is equal to one. In our case, it was taken equal to 1.5, providing excellent results. The choice of this value is not arbitrary. In fact, it is related to the Stress Factor, indicated as $SF$ or $K$. These two values are linked through the equations interpolated starting from the graph of the ref [8], shown below:

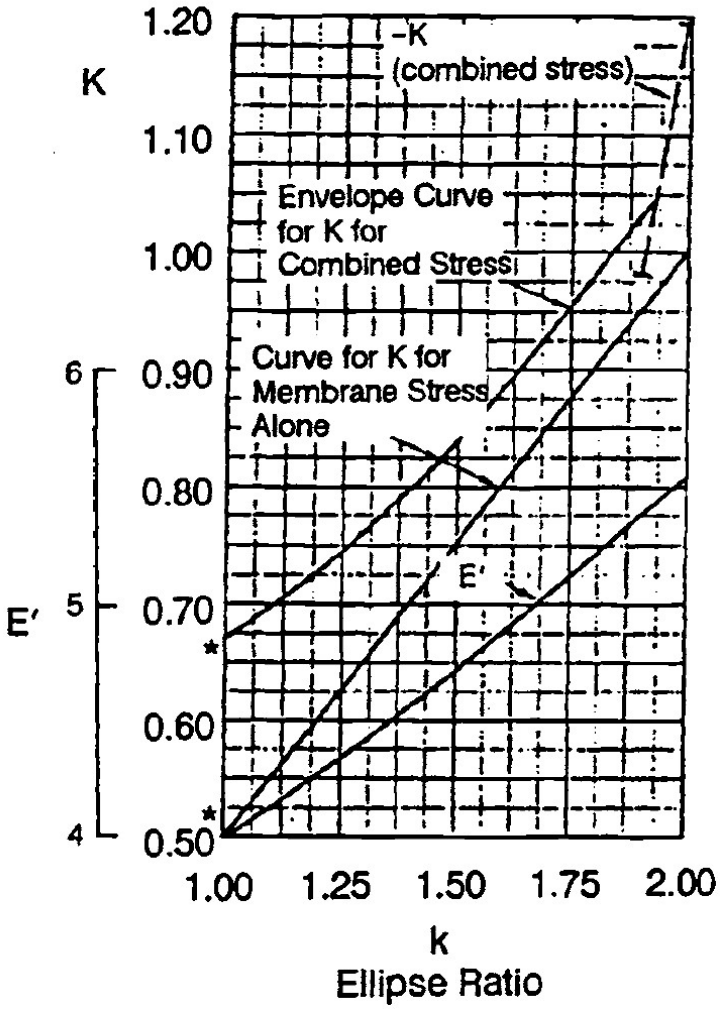


Figure 13: Safety factor in funtion of the Ellipse Ratio.

In turn, the stress factor is necessary for the calculation of the thickness of the ellipsoidal shells. In fact, in this case, the thickness cannot be calculated merely as in the case of a spherical shells but will be directly proportional to this value of $SF$ which considers the presence of combined membranes, discontinuities, and local stresses due to the internal pressure of the tank [8].
The thickness of this type of shell is obtained by averaging between the knuckle thickness and the crown, the formulas of which are given below [8]

$$s_k = \frac{K p_t a}{\sigma_{Max} e_w} \tag{50}$$

$$s_{cr} = \frac{p_t a}{2\sigma_{Max} e_w} \tag{51}$$

$$s_{eq} = \frac{(t_k + t_{cr})}{2} \tag{52}$$

Where $K$, $p_t$, $a$, and $\sigma_{Max}$ are defined above, while $e_w$ is the weld efficiency that can be defined as the reliability that can be obtained from the joints after welding. A joint efficiency of 1, which is the value used in this thesis work, indicates that the weld has the same strength as the base metal and is assumed to be seamless.
Higher $ER$ values lead to higher $K$ values (even above the unit) which lead to a greater knuckle thickness with a consequent increase in the average thickness and therefore, with the same $\sigma_{Max}$, greater structural strength, paying with an increase in the weight of the tank. On the contrary, $ER$ values lower than 1.5 lead to lower values of the knuckle thickness, and therefore of the average thickness of the shell, leading

to a reduction in the structural strength, with a fixed sigma, but also a reduction in the overall weight of the tank. To find a compromise between structural advantages and advantages in terms of weight, and therefore economics, the intermediate value of 1.5 was chosen.
This thickness will be slightly different from that of the cylindrical part of the tank; the latter, as well as the remaining thicknesses, were calculated using the same formula used in the reference case [7].
The value of $a$ used in the previous formula, is the value obtained downstream of the iterative: in this new version of the code, the iterative of the reference case has been replaced by Newton's method (also called the tangent method), which generates a succession of points starting from an initial point 0 which after a certain number of iterations converges to an approximation of the root of the function. This method was chosen because at each iteration it performs only one function evaluation, therefore it has a low computational cost. The same method here describe is used for all the geometries of the new version of the code.
Finally, in the reference case, the quantity that we tried to obtain with the iterative was unique; in this case, however, the quantities that were calculated through the iterative were two but linked as previously said.
After the iterative process, i.e. found the values of the height and the radius of the shells that returned a Rocket's length to diameter ratio equal to 10, the following other quantities were calculated:

- Volume of the cylindrical part of the tank: it is calculated starting from the volume of the tank, calculated as in the reference case, and from the volume of the ellipsoidal shells

$$V_{cylinder} = V_{tank} - V_{shells} \tag{53}$$

with

$$V_{shells} = \frac{4}{3}\pi a^2 b \tag{54}$$

- Rocket's length: is thus calculated

$$L_{rocket} = l_{grain} + l_{cyl} + l_{nozzle} + 2 \bullet b \tag{55}$$

where $l_{grain}$, $l_{cyl}$ and $l_{nozzle}$ are defined above, while $b$ is the height of the ellipsoidal shell. Also, the sum $l_{cyl} + 2 \bullet b$ is the tank total length.

- Rocket's diameter: in the new version of the code, the calculation of this quantity has been refined by adding to the contributions presented in the reference case, the contribution of the thickness of the liner, taken equal to the thickness of the cylindrical section of the tank. Consequentially

$$r_{rocket} = r_{tank} + s_{case} + s_{tank} + s_{lin} -> D_{rocket} = 2 \bullet r_{rocket} \tag{56}$$

- Tank masses: the masses of this geometry are calculated, for the vast majority, as in the reference case. The only mass calculated differently is that of the tank due to the change in geometry of the shells. Consequently, the formula relating to this last quantity is reported

$$m_{shells} = 2 \bullet (V_{tank}\rho_{materials}) \frac{E^{'}}{ER} \tag{57}$$

where $E^{'}$ is a corrective design parameter [8]. This can be calculated through the interpolation of the graph in figure 12, in which its dependence on the ellipse ratio is noted, or through the following equation [8]:

$$E^{'} = 2ER + \frac{1}{\sqrt{(ER)^2 - 1}} ln\left(\frac{ER + \sqrt{(ER)^2 - 1}}{ER - \sqrt{(ER)^2 - 1}}\right) \tag{58}$$

Then, adding this mass to that of the cylindrical section of the tank, the dry masses and the payload mass were calculated, as done in the reference case. Compared to the reference case, in the calculation of these quantities only the dry masses change. These will be more precise than those previously calculated, as they will also contain the contribution of the Liner mass ($m_{lin}$).

The values before and after the optimization process, relating to this first geometry, will be reported in the next chapter in conjunction with the materials selected for the new version of the code.

### 3.2.2 Cylindrical tank with spherical shells

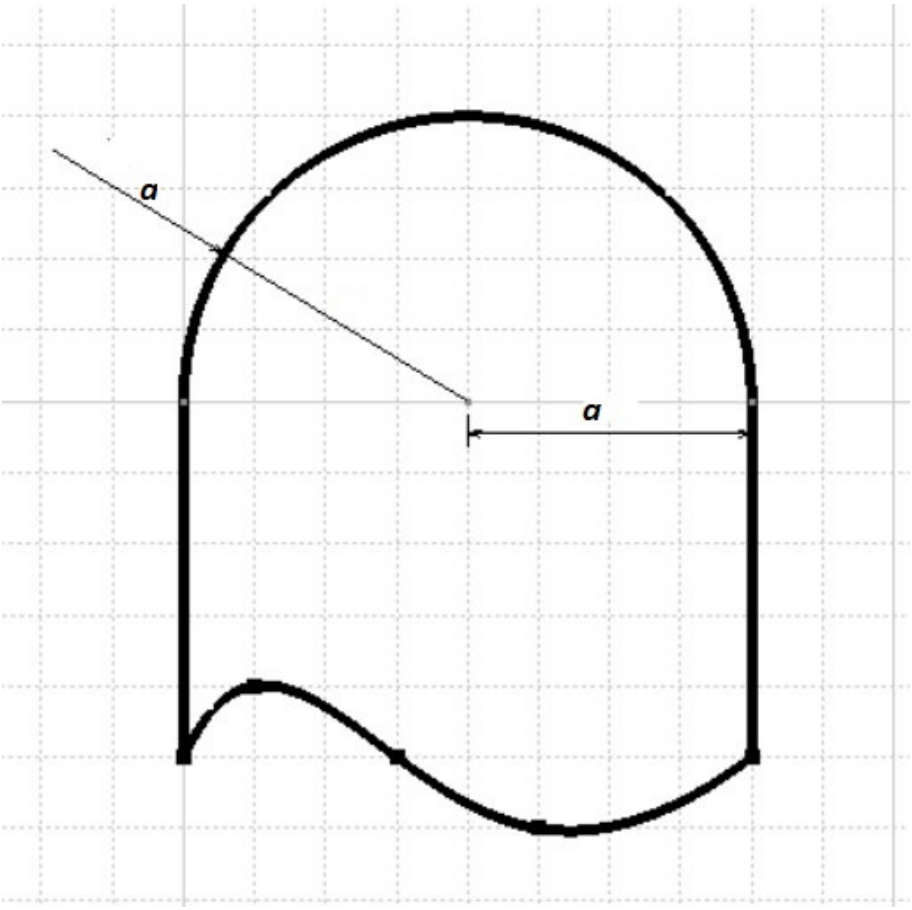


Figure 14: Sketch of the cylindrical tank with spherical shells.

The geometry used in this second case is practically identical to that of the Reference case [7]. However, the results that will be presented in the next chapter will be different in the case of coupling with aluminium alloy. This is for a few reasons:

- In the case of Reference [7], the pressure is used for the calculation of the geometric quantities as indicated in the Input data. Instead, in this case, this pressure is updated with the contribution of the fluid column. This is to ensure that the tank is sized in such a way as to structurally resist the expected external pressure loads.

- The second difference regards the iterative process used. As previously said, in all the new versions of the code the Newton method is used, which therefore replaces the previous method used in the Reference case [7].

- The last difference concerns specifically the coupling of this geometry with the aluminium alloy. In the case of Reference, a generic aluminium alloy is used which has a higher sigma than that of the alloy selected in the new version of the code, i.e. the DURAL. This involves variations on the calculation of the thicknesses and other quantities and, therefore, the reference case and the new case would be different even if the previous two points did not exist.

Instead, what has been said in the case of reference for the input parameters and for the equations used in the definition of the design quantities remains valid. The only equation that varies slightly is that of dry masses in which, this time, the contribution of the liner is also considered.

### 3.2.3 Cylindrical tank with trucated cone shells

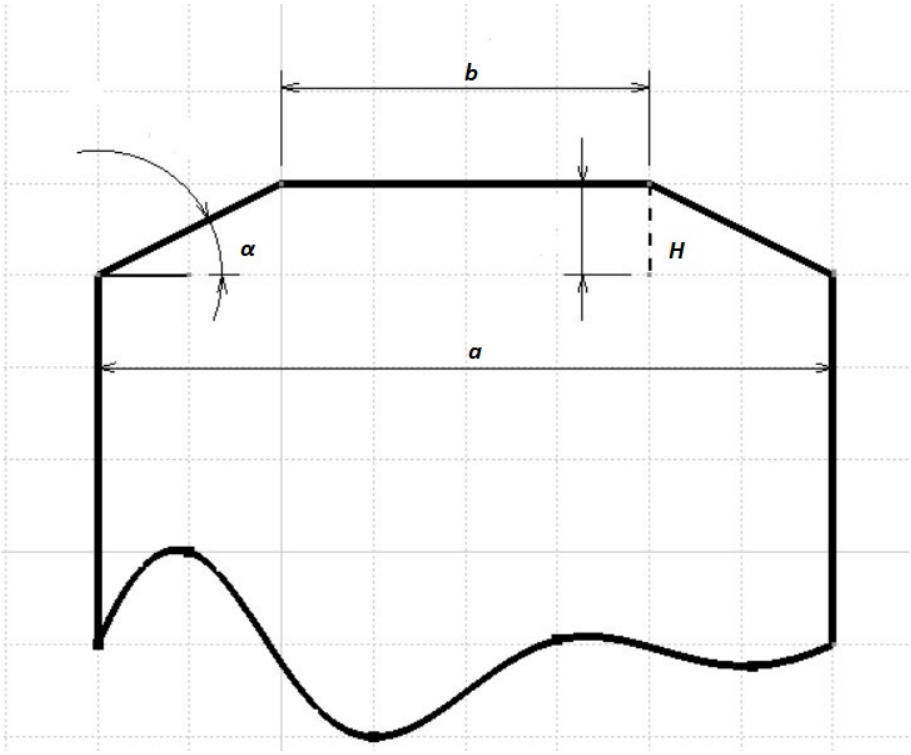


Figure 15: Sketch of the cylindrical tank with truncated cone shells.

In this last subsection of Chapter 3, the cylindrical tank with truncated cone shells is presented [8]. The same input parameters as the previous ones were used for this geometry. At the design level, the following assumptions, and the following equations were used:

- The initial radius of the tank ($a$) is assumed to be equal to the external radius of the grain ($r_{g_f}$) and it is assumed that the radius at the height of the truncation ($b$) is equal to half the radius at the base of the truncated cone. The height of the truncated cone($H$ or $H_{trunc}$), on the other hand, is calculated assuming an inclination angle of 30° and from trigonometry, we find that

$$H_{trunc} = (a - b)\, tan\alpha \tag{59}$$

  These quantities will vary downstream of Newton's iterative method previously described, to satisfy the $(L/D)_{rocket}$ constraint equal to 10.

- Tank volume: this quantity is calculated starting from the estimate of the tank volume as done in the case of Reference [7]. The volume of the shells, calculated with the following equation, allows the calculation of the volume of the cylindrical part of the tank by subtracting the volume of the caps from the estimated total volume of the tank

$$V_{shells} = \frac{2}{3}\pi H_{trunc}(a^2 + b^2 + a \bullet b) \tag{60}$$

$$V_{cyl-tank} = V_{tank} - V_{shells} \tag{61}$$

  Since the volume of the shells depends on the dimensions of the truncated cone, the real volume of the tank will be that obtained downstream of Newton's iterative method. This time the quantities that vary with the iterative are 4, but all are related to the base radius of the cone ($a$).

- After the end of the iterative method, the height of the trunk of the cone, the elongation of the cylindrical section of the tank, and the volumes mentioned above are calculated by using the new value of $a$.

- Thickness of the truncated cone shells: the thickness of this portion of the tank is calculated as follows [8]

$$s_{tc} = \frac{P_t a}{cos(\alpha)\sigma_{Max} e_W} \tag{62}$$

- Tank masses: through the thickness of the shells, we are able to calculate the weight of these

$$m_{shells} = 2 \bullet (A_{shells} s_{tc} \rho_{material}) \tag{63}$$

where $A_{shells}$ is the shells surfaces, calculated as

$$A_{shells} = 2 \bullet \left( \pi(a+b)\sqrt{H_{trunc}^2 + (a-b)^2} + \pi(a^2+b^2) \right) \tag{64}$$

For the calculation of the mass of the cylindrical portion of the tank the same procedure was used but adapting the formulas to the geometry

$$m_{cyl} = (A_{cyl} s_{tank} \rho_M) \tag{65}$$

where $A_{cyl}$ is the shells surfaces, calculated as

$$A_{cyl} = 2\pi a l_{cyl} \tag{66}$$

Finally, the mass of the nozzle and the liner were calculated, so that the dry masses could be calculated as done in section 3.2.1. The calculation of the dry masses allows us to obtain the payload mass and the final mass at the end of the trajectory with the same equations used for the previous geometries.

- Rocket's length: is thus calculated

$$L_{rocket} = l_{grain} + l_{cyl} + l_{nozzle} + 2 \bullet H_{trunc} \tag{67}$$

where $l_{grain}$, $l_{cyl}$ and $l_{nozzle}$ are defined above, while $H_{trunc}$ is the height of the ellipsoidal shell. Also, the sum $l_{cyl} + 2 \bullet H_{trunc}$ is the tank total length.

- Rocket's diameter: in the new version of the code, the calculation of this quantity has been refined by adding to the contributions presented in the reference case, the contribution of the thickness of the liner, taken equal to the thickness of the cylindrical section of the tank. Consequentially

$$r_{rocket} = r_{tank} + s_{case} + s_{tank} + s_{lin} -> D_{rocket} = 2 \bullet r_{rocket} \tag{68}$$

Everything that has been said about these quantities in the previous sections remains valid.

# 4 Optimization results and analysis

The previous chapter described the Reference case [7] and the new cases, with a particular focus on the new geometries [8] used and on the changes related to the new iterative process, providing a detailed description of what the new mathematical model of the code is. Furthermore, the hypotheses relating to the design of the new geometries are listed.
In this new section, the optimization process began with the scope of determining the best geometry-material couple. The first part of this chapter is divided into four sub-chapters, one for each material tested, and each chapter contains a chapter for each geometry. Finally, the best couple was identified and the analysis was carried out on it.

## 4.1 Material considered: Titanium 6Al-4

The first material tested is the Ti 6AL-4V, sometimes called TC4 or ASTM Grade 5, that is an alpha-beta titanium alloy with excellent corrosion resistance, high strength at low to moderate temperatures (up to approximately $350 - 400\,°C$, but properly treated they work well up to approximately $800\,°C$) and light weight. Thanks to these properties this material may be used in applications like aircraft turbine engine components, aircraft structural components, aerospace fasteners and some more fields, other than that of interest [12]. Also, high-cycle fatigue limits for Ti 6AL-4V are greatly influenced by both microstructure and surface conditions [11]. Some particular treatments are used to improve damage tolerance; these treatments are, for instance, stress relieving for formed or welded parts, and beta annealing. In any case, the material tends to behave well with fatigue. In the following table, the main properties are shown, as reported in the reference Handbook [11]:

| Properties | Values |
|---|---|
| Modulus of Elasticity $[MPa]$ | 104000 |
| Ultimate tensile strength $[MPa]$ | 900 |
| Yield strength $[MPa]$ | 880 |
| Density $[kg/m^3]$ | 4512 |
| Percentage elongation at the ultimate point (point break) | $10 - 16\%$ |

Table 3: Main features of Titanium 6Al-4.

The main problem with this kind of alloy is connected to the high costs.

### 4.1.1 Cylindrical tank with ellipsoidal shells

A cylindrical tank with an ellipsoidal shells is considered in this first case. The initial input parameters and the process used in new version of the code is being defined in the previous chapter and so they will not be reported here. Instead, the new optimal design and the main quantities obtained from the optimization are shown below. So, after the optimization, the code has found out the optimal design, which are:

1. Ullage volume, equal to $V_{g_i} = 0.35\,m^3$;

2. Mixture ratio, $\alpha = 1.74$.

In the first column of the following table is reported the performance evaluated with the input parameters of the reference case [7], i.e. the one reported in Section 3.2.1, considering the cylindrical tank with ellipsoidal shells made in Titanium 6AL-4 (Ell-Ti) [9], [11]. On the other hand, the second column reports the launcher characteristic and performance for the optimized design obtained for the same material/geometry combination. The values obtained from the reference case, on the other hand, were presented in section 1 of the third chapter, and therefore are not reported here.

| | Symbols | Initial results | Post-Optimization results |
|---|---|---|---|
| Propellant mass $[kg]$ | $m_{prop}$ | 438.4 | 435.2 |
| Fuel mass $[kg]$ | $m_{fuel}$ | 138.1 | 140.6 |
| Oxidiant mass $[kg]$ | $m_{ox}$ | 300.3 | 294.5 |
| Pressurizing gas mass $[kg]$ | $m_{gas}$ | 1.1 | 1.6 |
| Total mass of the tank $[kg]$ | $m_{tank}$ | 2.48 | 2.9 |
| Combustion chamber mass $[kg]$ | $m_{cc}$ | 9.1 | 9.5 |
| Nozzle mass $[kg]$ | $m_{nozzle}$ | 10.3 | 9.4 |
| Mass of the case $[kg]$ | $m_{case}$ | 20.5 | 22.6 |
| Liner mass $[kg]$ | $m_{lin}$ | 1.9 | 2.3 |
| Dry Mass 1 $[kg]$ | $m_{dry1}$ | 273.2 | 289.9 |
| Dry Mass 2 $[kg]$ | $m_{dry2}$ | 136.6 | 144.9 |
| Dry Mass 3 $[kg]$ | $m_{dry3}$ | 45.5 | 48.3 |
| Tank volume $[m^3]$ | $V_{tank}$ | 0.5 | 0.6 |
| Tank radius $[m]$ | $r_{tank}$ | 0.24 | 0.25 |
| Rocket's diameter $[m]$ | $D_{rocket}$ | 0.49 | 0.51 |
| Thickness of the tank $[mm]$ | $s_{tank}$ | 0.1 | 0.1 |
| Combustion chamber thickness $[mm]$ | $s_{case}$ | 0.03 | 0.03 |
| Liner thickness $[mm]$ | $s_{lin}$ | 0.08 | 0.09 |
| Tank lenght $[m]$ | $l_{tank}$ | 3.1 | 3.3 |
| Nozzle lenght $[m]$ | $L_{nozzle}$ | 0.64 | 0.6 |
| Rocket's total lenght $[m]$ | $L_{rocket}$ | 4.8 | 5.1 |
| Payload mass $[kg]$ | $m_{payload}$ | 75.4 | 79.6 |
| Final mass (payload+dry) $[kg]$ | $m_F$ | 120.9 | 127.9 |

Table 4: Ell-Ti

This material has a high density, and consequently, at a fixed volume, the weights of the various components will be greater than those with lower density (such as carbon fibre or aluminium alloy). This could lead to the belief that this material is therefore not suitable to perform the functions for which it is being designed; on the other hand, the high resistance to stress, i.e. high sigma values, lead to a reduction in the thickness values [12]

$$s_{components} = (P_{ref} \bullet r) / \sigma_{Max}$$

where $P_{ref}$ is the internal pressure of the components ($P_t$ if the component is the tank or $P_c$ if the component is the combustion chamber), $r$ is the component's radius, and $\sigma_{Max}$ is the minimum value between:

- The ultimate tensile strength

  $$\sigma_{ultimate} = C_{ultimate} \bullet \sigma_{ultimate_i}$$

  where $C_{ultimate}$ is a safety coefficient equal to 1.5, and $\sigma_{ultimate_i}$is the tabulate value of the ultimate tensile strength [12].

- The yield strength

  $$\sigma_y = C_y \bullet \sigma_{y_i}$$

  where $C_y$ is a safety coefficient equal to 1.25, and $\sigma_{y_i}$is the tabulate value of the yield strength [12].

Consequently, the final weight of the components will be smaller than one might think. Hence, this type of material is very useful when high mechanical performance is required and one is not interested in having the lowest possible weight.
An excellent method for a more accurate structural evaluation between materials could be to compare their specific strength values, i.e. the breakdown stress divided by the density ($\sigma_{Max}/\rho_M$), and the specific modulus, i.e. young's module on density ($E/\rho_M$) [12]. The first ratio, in fact, indicates how much weight the structure must bear to have a certain sturdiness. Therefore, for the same weight, it indicates whether the material is more or less robust than another. The specific modulus, on the other hand, is indicative of how much weight I can bear to have a certain structural stiffness. In fact, the bending

stiffness can be considered in the first analysis equal to $D = EI$, where $I$ is the moment of inertia of the structure, and, with the same $I$, if Young's modulus increases, the stiffness of the structure also increases [12]. Therefore, materials with high values of these ratios are of particular interest.
Beyond this analysis, a cost analysis is required. Basically, the most performing materials in the aeronautical field would be high-strength steels and titanium alloys (which have high values of specific modules and specific strength). To these, however, aluminium alloys are preferred precisely because of the high costs of the previous ones. This argument turns out to be valid and of particular importance even in the face of the design choice that will be made later: downstream of the choice of the best geometry-material pair, it is not certain that this would be the one used for certain applications, as it will probably turn out to be a very expensive choice, both for the cost of the materials themselves and for the costs of the processes necessary to make the structure with that material.
Finally, as can be seen from the previous table, the use of high-performance materials has resulted in extremely small thickness values. These are the minimum values to withstand the internal stresses due to the pressures, but it is not certain that they will be compatible with the selected production process or for the costs foreseen in a potential preliminary phase of the project. Consequently, a trade-off between these values and these considerations could lead to the choice of thicknesses greater than these to the detriment of the overall performance of the rocket, that is to the detriment of the payload mass.

### 4.1.2 Cylindrical tank with spherical shells

In this second case, a cylindrical tank with spherical shells is considered. As mentioned above, this is not the same as that of Reference [7]. The differences between the two were stated in section 3.2.2 and therefore will not be repeated here. Also in this case the initial input parameters and the process used in the new version of the code have been defined in the previous chapter and therefore will not be reported here. Instead, the following are the new input parameters and the main quantities obtained from the optimization. So, after the optimization, the code has found out the optimal design, which are:

1. Ullage volume, $V_{g_i} = 0.33\,m^3$;
2. Mixture ratio, equal to 1.75.

In the first column of the following table is reported the performance evaluated with the input parameters of the reference case [7], i.e. the one reported in Section 3.2.2, considering the cylindrical tank with spherical shells made in Titanium 6AL-4 (Sph-Ti) [9], [11]. On the other hand, the second column reports the launcher characteristic and performance for the optimized design obtained for the same material/geometry combination. The values obtained from the reference case, on the other hand, were presented in section 1 of the third chapter, and therefore are not reported here.

| | Symbols | Initial results | Post-Optimization results |
|---|---|---|---|
| Propellant mass $[kg]$ | $m_{prop}$ | 437.3 | 434.3 |
| Fuel mass $[kg]$ | $m_{fuel}$ | 137.7 | 140 |
| Oxidiant mass $[kg]$ | $m_{ox}$ | 299.6 | 294.3 |
| Pressurizing gas mass $[kg]$ | $m_{gas}$ | 1.1 | 1.5 |
| Total mass of the tank $[kg]$ | $m_{tank}$ | 2.2 | 2.6 |
| Combustion chamber mass $[kg]$ | $m_{cc}$ | 9.1 | 9.4 |
| Nozzle mass $[kg]$ | $m_{nozzle}$ | 10.3 | 9.4 |
| Mass of the case $[kg]$ | $m_{case}$ | 20.1 | 21.9 |
| Liner mass $[kg]$ | $m_{lin}$ | 3.9 | 4.6 |
| Dry Mass 1 $[kg]$ | $m_{dry1}$ | 280.7 | 297.1 |
| Dry Mass 2 $[kg]$ | $m_{dry2}$ | 140.3 | 148.6 |
| Dry Mass 3 $[kg]$ | $m_{dry3}$ | 46.8 | 49.5 |
| Tank volume $[m^3]$ | $V_{tank}$ | 0.51 | 0.59 |
| Tank radius $[m]$ | $r_{tank}$ | 0.23 | 0.25 |
| Rocket's diameter $[m]$ | $D_{rocket}$ | 0.48 | 0.5 |
| Thickness of the tank $[mm]$ | $s_{tank}$ | 0.1 | 0.1 |
| Combustion chamber thickness $[mm]$ | $s_{case}$ | 0.03 | 0.03 |
| Liner thickness $[mm]$ | $s_{lin}$ | 0.01 | 0.01 |
| Tank lenght $[m]$ | $l_{tank}$ | 2.5 | 2.6 |
| Nozzle lenght $[m]$ | $L_{nozzle}$ | 0.6 | 0.6 |
| Rocket's total lenght $[m]$ | $L_{rocket}$ | 4.8 | 5 |
| Payload mass $[kg]$ | $m_{payload}$ | 73.3 | 76.7 |
| Final mass (payload+dry) $[kg]$ | $m_F$ | 120.1 | 126.3 |

Table 5: Sph-Ti

The considerations made for the previous geometry remain valid as both are made of the same material. What stands out is the fact that when passing from ellipsoidal to cylindrical shell the performance drops slightly. This is because the assumptions made regarding the ellipsoidal shell ($H_{trunc} = a/ER$ where these quantities are defined in the previous chapter) lead these to contain a greater quantity of propellant than that contained in the spherical one.

### 4.1.3 Cylindrical tank with truncated cone shells

Finally, a cylindrical tank with truncated cone shells is considered in this third case. The initial input parameters and the process used in new version of the code is being defined in the previous Chapter and so they will not be reported here. Instead, the new optimal design and the main quantities obtained from the optimization are shown below. So, after the optimization, the code has found out the optimal design, which are:

1. Ullage volume, $V_{g_i} = 0.33\,m^3$;
2. Mixture ratio, equal to 1.75.

In the first column of the following table is reported the performance evaluated with the input parameters of the reference case [7], i.e. the one reported in Section 3.2.3, considering the cylindrical tank with truncated cone shells made in Titanium 6AL-4 (Tc-Ti) [9], [11]. On the other hand, the second column reports the launcher characteristic and performance for the optimized design obtained for the same material/geometry combination. The values obtained from the reference case, on the other hand, were presented in section 1 of the third chapter, and therefore are not reported here.

| | Symbols | Initial results | Post-Optimization results |
|---|---|---|---|
| Propellant mass $[kg]$ | $m_{prop}$ | 438.8 | 435.7 |
| Fuel mass $[kg]$ | $m_{fuel}$ | 138.2 | 140.7 |
| Oxidiant mass $[kg]$ | $m_{ox}$ | 300.6 | 294.9 |
| Pressurizing gas mass $[kg]$ | $m_{gas}$ | 1.1 | 1.5 |
| Total mass of the tank $[kg]$ | $m_{tank}$ | 2.7 | 3.2 |
| Combustion chamber mass $[kg]$ | $m_{cc}$ | 9.1 | 9.4 |
| Nozzle mass $[kg]$ | $m_{nozzle}$ | 10.3 | 9.4 |
| Mass of the case $[kg]$ | $m_{case}$ | 19.5 | 21.4 |
| Liner mass $[kg]$ | $m_{lin}$ | 2.1 | 2.5 |
| Dry Mass 1 $[kg]$ | $m_{dry1}$ | 269.7 | 286.3 |
| Dry Mass 2 $[kg]$ | $m_{dry2}$ | 134.8 | 143.1 |
| Dry Mass 3 $[kg]$ | $m_{dry3}$ | 44.9 | 47.7 |
| Tank volume $[m^3]$ | $V_{tank}$ | 0.51 | 0.59 |
| Tank radius $[m]$ | $r_{tank}$ | 0.23 | 0.24 |
| Rocket's diameter $[m]$ | $D_{rocket}$ | 0.48 | 0.49 |
| Thickness of the tank $[mm]$ | $s_{tank}$ | 0.1 | 0.1 |
| Combustion chamber thickness $[mm]$ | $s_{case}$ | 0.03 | 0.3 |
| Liner thickness $[mm]$ | $s_{lin}$ | 0.07 | 0.08 |
| Tank lenght $[m]$ | $l_{tank}$ | 2.9 | 3 |
| Nozzle lenght $[m]$ | $L_{nozzle}$ | 0.6 | 0.6 |
| Rocket's total lenght $[m]$ | $L_{rocket}$ | 4.7 | 5 |
| Payload mass $[kg]$ | $m_{payload}$ | 76.7 | 80.7 |
| Final mass (payload+dry) $[kg]$ | $m_F$ | 121.7 | 128.4 |

Table 6: Tc-Ti

In addition, the pre-optimization quantities are reported, to make the comparison between the initial situation and the optimized one immediately. The considerations made for the ellipsoidal tank remain valid as both are made of the same material. What stands out is the fact that when passing from ellipsoidal to truncated cone shell the performance grows up slightly. The optimized design calculates a higher mass of fuel than the non-optimized case, but a lower oxidant mass. This leads to an increase in terms of payload mass despite the higher Dry masses. Therefore, what can be noted through this first analysis with fixed geometry and varying quantities, is that the fixed mass of propellant, imposed by the mission, can involve significant increases in the mass of transportable payloads, only by varying geometry, through a trade-off between the various quantities involved.

## 4.2 Material considered: Dural (Al-2024)

The 2024 Duralumin, usually named Dural, is an aluminium alloy, with copper as the primary alloying element [12]. Specifically, this material is formed for $90 - 93\%$ of aluminium, while copper is present in a percentage between $4 - 5\%$. Other elements are present in lower percentages like, for instance, zinc, magnesium and manganese (overall not over the $3 - 4$). Those are added to improve some features like weldability. Thanks to these properties, Dural is commonly used in the aerospace field for the majority of the structural elements. In the following table, the main properties are shown:

| Properties | Values |
|---|---|
| Modulus of Elasticity $[MPa]$ | 73100 |
| Ultimate tensile strength $[MPa]$ | 469 |
| Yield strength $[MPa]$ | 324 |
| Density $[kg/m^3]$ | 2780 |
| Percentage elongation at the ultimate point (point break) | $14 - 20\%$ |

Table 7: Main features of Dural (Al-2024).

In previously years, the main defect was the welding of this alloy, but nowadays the problem has been overcome through the use of specific processing techniques. At present, the low corrosion resistance involves easy oxidation of the material, making the material more brittle than pure aluminium. It is therefore necessary to treat the surfaces of these alloys to prevent oxygen to come into contact with the alloy [12].

### 4.2.1 Cylindrical tank with ellipsoidal shells

A cylindrical tank with an ellipsoidal shells is considered in this first case. The initial input parameters and the process used in new version of the code is being defined in the previous chapter and so they will not be reported here. Instead, the new optimal design and the main quantities obtained from the optimization are shown below. So, after the optimization, the code has found out the optimal design, which are:

1. Ullage volume, equal to $V_{g_i} = 0.33\, m^3$;

2. Mixture ratio, equal to $\alpha = 1.74$.

In the first column of the following table is reported the performance evaluated with the input parameters of the reference case [7], i.e. the one reported in Section 3.2.1, considering the cylindrical tank with ellipsoidal shells made in Dural (Al-2024) (Ell-Al) [9], [12]. On the other hand, the second column reports the launcher characteristic and performance for the optimized design obtained for the same material/geometry combination. The values obtained from the reference case, on the other hand, were presented in section 1 of the third chapter, and therefore are not reported here.

| | Symbols | Initial results | Post-Optimization results |
|---|---|---|---|
| Propellant mass $[kg]$ | $m_{prop}$ | 436.8 | 433.8 |
| Fuel mass $[kg]$ | $m_{fuel}$ | 137.6 | 140.3 |
| Oxidiant mass $[kg]$ | $m_{ox}$ | 299.2 | 293.4 |
| Pressurizing gas mass $[kg]$ | $m_{gas}$ | 1.1 | 1.5 |
| Total mass of the tank $[kg]$ | $m_{tank}$ | 3.5 | 4.1 |
| Combustion chamber mass $[kg]$ | $m_{cc}$ | 9.2 | 9.5 |
| Nozzle mass $[kg]$ | $m_{nozzle}$ | 10.3 | 9.4 |
| Mass of the case $[kg]$ | $m_{case}$ | 20.5 | 22.3 |
| Liner mass $[kg]$ | $m_{lin}$ | 2.7 | 3.1 |
| Dry Mass 1 $[kg]$ | $m_{dry1}$ | 284.6 | 300.6 |
| Dry Mass 2 $[kg]$ | $m_{dry2}$ | 142.3 | 150.3 |
| Dry Mass 3 $[kg]$ | $m_{dry3}$ | 47.4 | 50.1 |
| Tank volume $[m^3]$ | $V_{tank}$ | 0.51 | 0.58 |
| Tank radius $[m]$ | $r_{tank}$ | 0.24 | 0.25 |
| Rocket's diameter $[m]$ | $D_{rocket}$ | 0.49 | 0.51 |
| Thickness of the tank $[mm]$ | $s_{tank}$ | 0.25 | 0.27 |
| Combustion chamber thickness $[mm]$ | $s_{case}$ | 0.08 | 0.08 |
| Liner thickness $[mm]$ | $s_{lin}$ | 0.24 | 0.2 |
| Tank lenght $[m]$ | $l_{tank}$ | 3.1 | 3.3 |
| Nozzle lenght $[m]$ | $L_{nozzle}$ | 0.6 | 0.6 |
| Rocket's total lenght $[m]$ | $L_{rocket}$ | 4.8 | 5 |
| Payload mass $[kg]$ | $m_{payload}$ | 71.9 | 75.4 |
| Final mass (payload+dry) $[kg]$ | $m_F$ | 119.4 | 125.5 |

Table 8: (Ell-Al)

In addition, the pre-optimization quantities are reported, to make the comparison between the initial situation and the optimized one immediately. This second material has a lower density than the first one, and consequently, the components will have a lower weight at a fixed volume. In the case presented in this thesis, the volume is not fixed and for this reason, the weight of the components is slightly greater. This is because the resistance of Dural is much lower (just under half) than the previous one, and consequently, the thicknesses will be much greater (about double) than those of the previous material. The sigma used in this case to calculate the thickness is obtained in the same way presented in the section relative to the first case. This weight increase leads to a reduction in the payload mass and this means that the selected material is unlikely to be this. This could have been expected since a material similar to the Dural was the material present in the base code, consequently, the other materials used were selected to exceed the performance obtained from Dural.

### 4.2.2 Cylindrical tank with spherical shells

In this second case, a cylindrical tank with spherical shells is considered. Also in this case the initial input parameters and the process used in the new version of the code have been defined in the previous chapter and therefore will not be reported here. Instead, the following are the new input parameters and the main quantities obtained from the optimization. So, after the optimization, the code has found out the optimal design, which are:

1. Ullage volume, $0.30\,m^3$;
2. Mixture ratio, 1.76.

In the first column of the following table is reported the performance evaluated with the input parameters of the reference case [7], i.e. the one reported in Section 3.2.2, considering the cylindrical tank with spherical shells made in Dural (Al-2024) (Sp-Al) [9], [12]. On the other hand, the second column reports the launcher characteristic and performance for the optimized design obtained for the same material/geometry combination. The values obtained from the reference case, on the other hand, were presented in section 1 of the third chapter, and therefore are not reported here.

| | Symbols | Initial results | Post-Optimization results |
|---|---|---|---|
| Propellant mass $[kg]$ | $m_{prop}$ | 435.2 | 432.4 |
| Fuel mass $[kg]$ | $m_{fuel}$ | 137.1 | 139.4 |
| Oxidiant mass $[kg]$ | $m_{ox}$ | 298.1 | 293 |
| Pressurizing gas mass $[kg]$ | $m_{gas}$ | 1.1 | 1.4 |
| Total mass of the tank $[kg]$ | $m_{tank}$ | 3.2 | 3.6 |
| Combustion chamber mass $[kg]$ | $m_{cc}$ | 9.2 | 9.5 |
| Nozzle mass $[kg]$ | $m_{nozzle}$ | 10.3 | 9.5 |
| Mass of the case $[kg]$ | $m_{case}$ | 20 | 21.5 |
| Liner mass $[kg]$ | $m_{lin}$ | 5.6 | 6.3 |
| Dry Mass 1 $[kg]$ | $m_{dry1}$ | 296.5 | 311.7 |
| Dry Mass 2 $[kg]$ | $m_{dry2}$ | 148.3 | 155.8 |
| Dry Mass 3 $[kg]$ | $m_{dry3}$ | 49.4 | 51.9 |
| Tank volume $[m^3]$ | $V_{tank}$ | 0.51 | 0.57 |
| Tank radius $[m]$ | $r_{tank}$ | 0.24 | 0.25 |
| Rocket's diameter $[m]$ | $D_{rocket}$ | 0.48 | 0.50 |
| Thickness of the tank $[mm]$ | $s_{tank}$ | 0.25 | 0.26 |
| Combustion chamber thickness $[mm]$ | $s_{case}$ | 0.08 | 0.08 |
| Liner thickness $[mm]$ | $s_{lin}$ | 0.21 | 0.22 |
| Tank lenght $[m]$ | $l_{tank}$ | 2.5 | 2.6 |
| Nozzle lenght $[m]$ | $L_{nozzle}$ | 0.6 | 0.6 |
| Rocket's total lenght $[m]$ | $L_{rocket}$ | 4.8 | 4.9 |
| Payload mass $[kg]$ | $m_{payload}$ | 68.5 | 71.1 |
| Final mass (payload+dry) $[kg]$ | $m_F$ | 117.9 | 123 |

Table 9: Sp-Al

The considerations relative to the first geometry are valid either for this second one. As seen for the first material, the performances of the cylindrical tank with a spherical shell are worst than those presented for the case with an ellipsoidal shell. The reason for this is explained in the same section of the previous material, so, it will not be reported here.

### 4.2.3 Cylindrical tank with truncated cone shells

Finally, a cylindrical tank with truncated cone shells is considered in this third case. The initial input parameters and the process used in new version of the code is being defined in the previous Chapter and so they will not be reported here. Instead, the new optimal design and the main quantities obtained from the optimization are shown below. So, after the optimization, the code has found out the optimal design, which are:

1. Ullage Volume, $V_{g_i} = 0.32\,m^3$;
2. Mixture Ratio, $\alpha = 1.75$.

In the first column of the following table is reported the performance evaluated with the input parameters of the reference case [7], i.e. the one reported in Section 3.2.3, considering the cylindrical tank with truncated cone shells made in Dural (Al-2024) (Tc-Al) [9], [12]. On the other hand, the second column reports the launcher characteristic and performance for the optimized design obtained for the same material/geometry combination. The values obtained from the reference case, on the other hand, were presented in section 1 of the third chapter, and therefore are not reported here.

| | Symbols | Initial results | Post-Optimization results |
|---|---|---|---|
| Propellant mass $[kg]$ | $m_{prop}$ | 437.2 | 434.2 |
| Fuel mass $[kg]$ | $m_{fuel}$ | 137.7 | 140.5 |
| Oxidiant mass $[kg]$ | $m_{ox}$ | 299.4 | 293.7 |
| Pressurizing gas mass $[kg]$ | $m_{gas}$ | 1.1 | 1.5 |
| Total mass of the tank $[kg]$ | $m_{tank}$ | 3.8 | 4.5 |
| Combustion chamber mass $[kg]$ | $m_{cc}$ | 9.2 | 9.6 |
| Nozzle mass $[kg]$ | $m_{nozzle}$ | 10.3 | 9.5 |
| Mass of the case $[kg]$ | $m_{case}$ | 19.5 | 21.1 |
| Liner mass $[kg]$ | $m_{lin}$ | 3.1 | 3.5 |
| Dry Mass 1 $[kg]$ | $m_{dry1}$ | 282.3 | 298 |
| Dry Mass 2 $[kg]$ | $m_{dry2}$ | 141.1 | 149 |
| Dry Mass 3 $[kg]$ | $m_{dry3}$ | 47 | 49.7 |
| Tank volume $[m^3]$ | $V_{tank}$ | 0.50 | 0.57 |
| Tank radius $[m]$ | $r_{tank}$ | 0.24 | 0.25 |
| Rocket's diameter $[m]$ | $D_{rocket}$ | 0.48 | 0.50 |
| Thickness of the tank $[mm]$ | $s_{tank}$ | 0.25 | 0.26 |
| Combustion chamber thickness $[mm]$ | $s_{case}$ | 0.08 | 0.08 |
| Liner thickness $[mm]$ | $s_{lin}$ | 0.24 | 0.25 |
| Tank lenght $[m]$ | $l_{tank}$ | 2.9 | 3 |
| Nozzle lenght $[m]$ | $L_{nozzle}$ | 0.6 | 0.6 |
| Rocket's total lenght $[m]$ | $L_{rocket}$ | 4.7 | 4.9 |
| Payload mass $[kg]$ | $m_{payload}$ | 72.9 | 76 |
| Final mass (payload+dry) $[kg]$ | $m_F$ | 120 | 125.7 |

Table 10: Tc-Al

In addition, the pre-optimization quantities are reported, to make the comparison between the initial situation and the optimized one immediately. Also in this case, refer to the previous sections about the reasons why this geometry is better than the one with ellipsoidal shells. All considerations relating to the reduction in performance due to material changes remain valid.

## 4.3 Material considered: INCONEL 718

The INCONEL alloy 718 is a high-strength, corrosion-resistant nickel chromium material with a chemical composition composed of $50-55$ of Nickel (usually plus cobalt), $17-21\%$ of Chromium and other elements like Iron, Niobium, etc. in a lower percentage. The best characteristic is the welding, especially its resistance to postweld cracking is outstanding. Furthermore, the ease and economy with which Inconel can be fabricated, in combination with good tensile, fatigue, creep, and rupture strength, have resulted in a wide range of applications. Some of these are components for fuelled rockets, rings, casings and various formed sheet metal parts for aircraft. In the following table, the main properties are shown, as reported in the reference Handbook [13]:

| Properties | Values |
|---|---|
| Modulus of Elasticity $[MPa]$ | 200000 |
| Ultimate tensile strength $[MPa]$ | 1375 |
| Yield strength $[MPa]$ | 1100 |
| Density $[kg/m^3]$ | 8190 |
| Percentage elongation at the ultimate point (point break) | $14-20\%$ |

Table 11: Main features of INCONEL 718.

### 4.3.1 Cylindrical tank with ellipsoidal shells

Again, a cylindrical tank with an ellipsoidal shell is considered in this first case. The initial input parameters and the process used in the subroutine "mass_dry" is being defined in the previous chapter and so they will not be reported here. Instead, the new input parameters and the main magnitudes obtained from the optimization are shown below. So, after the optimization, the code has calculated the new inputs that are:

1. Ullage Volume equal to $0.34\,m^3$;

2. Mixture Ratio equal to 1.74.

In the first column of the following table is reported the performance evaluated with the input parameters of the reference case [7], i.e. the one reported in Section 3.2.1, considering the cylindrical tank with ellipsoidal shells made in INCONEL alloy 718 (Ell-Inc) [9], [13]. On the other hand, the second column reports the launcher characteristic and performance for the optimized design obtained for the same material/geometry combination. The values obtained from the reference case, on the other hand, were presented in section 1 of the third chapter, and therefore are not reported here.

| | Symbols | Initial results | Post-Optimization results |
|---|---|---|---|
| Propellant mass $[kg]$ | $m_{prop}$ | 437.6 | 434.5 |
| Fuel mass $[kg]$ | $m_{fuel}$ | 137.8 | 140.5 |
| Oxidiant mass $[kg]$ | $m_{ox}$ | 299.7 | 293.9 |
| Pressurizing gas mass $[kg]$ | $m_{gas}$ | 1.1 | 1.5 |
| Total mass of the tank $[kg]$ | $m_{tank}$ | 3.1 | 3.6 |
| Combustion chamber mass $[kg]$ | $m_{cc}$ | 9.1 | 9.5 |
| Nozzle mass $[kg]$ | $m_{nozzle}$ | 10.3 | 9.4 |
| Mass of the case $[kg]$ | $m_{case}$ | 20.5 | 22.4 |
| Liner mass $[kg]$ | $m_{lin}$ | 2.4 | 2.8 |
| Dry Mass 1 $[kg]$ | $m_{dry1}$ | 279.5 | 295.9 |
| Dry Mass 2 $[kg]$ | $m_{dry2}$ | 139.7 | 147.9 |
| Dry Mass 3 $[kg]$ | $m_{dry3}$ | 46.6 | 49.3 |
| Tank volume $[m^3]$ | $V_{tank}$ | 0.52 | 0.59 |
| Tank radius $[m]$ | $r_{tank}$ | 0.24 | 0.25 |
| Rocket's diameter $[m]$ | $D_{rocket}$ | 0.48 | 0.50 |
| Thickness of the tank $[mm]$ | $s_{tank}$ | 0.07 | 0.08 |
| Combustion chamber thickness $[mm]$ | $s_{case}$ | 0.02 | 0.02 |
| Liner thickness $[mm]$ | $s_{lin}$ | 0.07 | 0.08 |
| Tank lenght $[m]$ | $l_{tank}$ | 3.1 | 3.3 |
| Nozzle lenght $[m]$ | $L_{nozzle}$ | 0.6 | 0.6 |
| Rocket's total lenght $[m]$ | $L_{rocket}$ | 4.9 | 5.1 |
| Payload mass $[kg]$ | $m_{payload}$ | 73.5 | 77.3 |
| Final mass (payload+dry) $[kg]$ | $m_F$ | 120.1 | 126.6 |

Table 12: Ell-Inc

INCONEL is a very performing material (its characteristics are very similar to those of titanium). It got very high values of stress at break and deformation, meaning that the thicknesses found for this material are among the lowest calculated. This prevents the weight of the tank from rising dramatically and at the same time allows for an extremely performing tank in terms of mechanical characteristics. The remaining considerations on the calculation of the thicknesses have been set out in the previous sections and, therefore, are not reported here.

### 4.3.2 Cylindrical tank with spherical shells

In this second case, a cylindrical tank with spherical shells is considered. Also in this case the initial input parameters and the process used in the new version of the code have been defined in the previous chapter and therefore will not be reported here. Instead, the following are the new input parameters and the main quantities obtained from the optimization. So, after the optimization, the code has found out the optimal design, which are:

1. Ullage Volume, $V_{g_i} = 0.32\,m^3$;
2. Mixture Ratio, $\alpha = 1.75$.

In the first column of the following table is reported the performance evaluated with the input parameters of the reference case [7], i.e. the one reported in Section 3.2.2, considering the cylindrical tank with spherical shells made in INCONEL alloy 718 (Sp-Inc) [9], [13]. On the other hand, the second column reports the launcher characteristic and performance for the optimized design obtained for the same material/geometry combination. The values obtained from the reference case, on the other hand, were presented in section 1 of the third chapter, and therefore are not reported here.

| | Symbols | Initial results | Post-Optimization results |
|---|---|---|---|
| Propellant mass $[kg]$ | $m_{prop}$ | 436.2 | 433.3 |
| Fuel mass $[kg]$ | $m_{fuel}$ | 137.4 | 139.7 |
| Oxidiant mass $[kg]$ | $m_{ox}$ | 298.8 | 293.6 |
| Pressurizing gas mass $[kg]$ | $m_{gas}$ | 1.1 | 1.5 |
| Total mass of the tank $[kg]$ | $m_{tank}$ | 2.8 | 3.2 |
| Combustion chamber mass $[kg]$ | $m_{cc}$ | 9.1 | 9.5 |
| Nozzle mass $[kg]$ | $m_{nozzle}$ | 10.3 | 9.5 |
| Mass of the case $[kg]$ | $m_{case}$ | 20 | 21.7 |
| Liner mass $[kg]$ | $m_{lin}$ | 4.9 | 5.6 |
| Dry Mass 1 $[kg]$ | $m_{dry1}$ | 289.5 | 305.3 |
| Dry Mass 2 $[kg]$ | $m_{dry2}$ | 144.7 | 152.69 |
| Dry Mass 3 $[kg]$ | $m_{dry3}$ | 48.3 | 50.9 |
| Tank volume $[m^3]$ | $V_{tank}$ | 0.51 | 0.58 |
| Tank radius $[m]$ | $r_{tank}$ | 0.24 | 0.25 |
| Rocket's diameter $[m]$ | $D_{rocket}$ | 0.48 | 0.50 |
| Thickness of the tank $[mm]$ | $s_{tank}$ | 0.07 | 0.08 |
| Combustion chamber thickness $[mm]$ | $s_{case}$ | 0.02 | 0.02 |
| Liner thickness $[mm]$ | $s_{lin}$ | 0.08 | 0.08 |
| Tank lenght $[m]$ | $l_{tank}$ | 2.5 | 2.7 |
| Nozzle lenght $[m]$ | $L_{nozzle}$ | 0.6 | 0.6 |
| Rocket's total lenght $[m]$ | $L_{rocket}$ | 4.8 | 5 |
| Payload mass $[kg]$ | $m_{payload}$ | 70.6 | 73.6 |
| Final mass (payload+dry) $[kg]$ | $m_F$ | 118.9 | 124.5 |

Table 13: Sp-Inc

The considerations relative to the first geometry are valid either for this second one. As seen for the first material, the performances of the cylindrical tank with a spherical shell are worst than those presented for the case with an ellipsoidal shells. The reason for this is explained in the same section of the first material, so, it will not be reported here.

### 4.3.3 Cylindrical tank with truncated cone shells

Finally, a cylindrical tank with truncated cone shells is considered in this third case. The initial input parameters and the process used in new version of the code is being defined in the previous Chapter and so they will not be reported here. Instead, the new optimal design and the main quantities obtained from the optimization are shown below. So, after the optimization, the code has found out the optimal design, which are:

1. Ullage Volume, $V_{g_i} = 0.33\,m^3$;
2. Mixture Ratio equal to 1.75.

In the first column of the following table is reported the performance evaluated with the input parameters of the reference case [7], i.e. the one reported in Section 3.2.3, considering the cylindrical tank with truncated cone shells made in INCONEL alloy 718 (Tc-Inc) [9], [13]. On the other hand, the second column reports the launcher characteristic and performance for the optimized design obtained for the same material/geometry combination. The values obtained from the reference case, on the other hand, were presented in section 1 of the third chapter, and therefore are not reported here.

| | Symbols | Initial results | Post-Optimization results |
|---|---|---|---|
| Propellant mass $[kg]$ | $m_{prop}$ | 437.9 | 434.9 |
| Fuel mass $[kg]$ | $m_{fuel}$ | 137.94 | 140.6 |
| Oxidiant mass $[kg]$ | $m_{ox}$ | 300 | 294.2 |
| Pressurizing gas mass $[kg]$ | $m_{gas}$ | 1.1 | 1.5 |
| Total mass of the tank $[kg]$ | $m_{tank}$ | 3.4 | 3.9 |
| Combustion chamber mass $[kg]$ | $m_{cc}$ | 9.1 | 9.5 |
| Nozzle mass $[kg]$ | $m_{nozzle}$ | 10.3 | 9.5 |
| Mass of the case $[kg]$ | $m_{case}$ | 19.5 | 21.3 |
| Liner mass $[kg]$ | $m_{lin}$ | 2.7 | 3.1 |
| Dry Mass 1 $[kg]$ | $m_{dry1}$ | 276.7 | 292.9 |
| Dry Mass 2 $[kg]$ | $m_{dry2}$ | 138.3 | 146.5 |
| Dry Mass 3 $[kg]$ | $m_{dry3}$ | 46.1 | 48.8 |
| Tank volume $[m^3]$ | $V_{tank}$ | 0.51 | 0.6 |
| Tank radius $[m]$ | $r_{tank}$ | 0.24 | 0.25 |
| Rocket's diameter $[m]$ | $D_{rocket}$ | 0.48 | 0.50 |
| Thickness of the tank $[mm]$ | $s_{tank}$ | 0.07 | 0.08 |
| Combustion chamber thickness $[mm]$ | $s_{case}$ | 0.03 | 0.03 |
| Liner thickness $[mm]$ | $s_{lin}$ | 0.08 | 0.08 |
| Tank lenght $[m]$ | $l_{tank}$ | 2.9 | 3.1 |
| Nozzle lenght $[m]$ | $L_{nozzle}$ | 0.6 | 0.6 |
| Rocket's total lenght $[m]$ | $L_{rocket}$ | 4.7 | 4.9 |
| Payload mass $[kg]$ | $m_{payload}$ | 74.7 | 78.1 |
| Final mass (payload+dry) $[kg]$ | $m_F$ | 120.8 | 126.9 |

Table 14: Tc-Inc

In addition, the pre-optimization quantities are reported, to make the comparison between the initial situation and the optimized one immediately. Also in this case, refer to the previous sections about the reasons why this geometry is better than the one with ellipsoidal shells. All considerations relating to the reduction in performance due to material changes remain valid.

## 4.4 Material considered: Carbon Fibre Composite

Baselines of Carbon Fiber are used in aerospace applications and have 30 years of production history, and are known for their balanced composite properties, high quality, consistency, reliability and supply ability. It's about a kind of material made of Carbon fibres (which resist only traction but not compression) with high properties, impregnated inside with resins (to provide compressive strength) [10].
In this way, a layer is obtained and the final product has a certain number of layers. From one layer to another the fibres can be oriented differently, allowing the designer to modify the mechanical characteristics of the laminate by changing the orientation of the fibres. The Carbon Fiber chosen for this thesis work is named CARBON/EPOXY T300/934 or more commonly named CYCOM 934 which is a high flow, $177\,°C$ curing epoxy resin with good $93\,°C$ wet and $177\,°C$ dry service capability. This material has some main features like availability in a broad range of fibres and forms including tape, fabric and roving, and, also, meets all NASA outgassing requirements. CYCOM 934 is used in a wide range of aerospace applications, for structural components and in both commercial and military fields [14]. Furthermore is used in critical space structures. For this specific material, the theory of the quasi-isotropic material is used and consequently, the membrane properties are isotropic and identical for each of the laminates. Moreover, the laminates have 33% fibre at 45° and 33% fibre at 0°. The main problems related to this type of material are:

- The high costs associated with the use of particular processes and the fact that the vast majority are still in the research phase.
- Fragility. These materials have high breaking stresses but have no residual capacity, i.e. they do not exhibit plastic behaviour (which is why their use is still limited).

In the following table, the main properties are shown, as reported in the reference Handbook [14]:

| Properties | Values |
|---|---|
| Modulus of Elasticity $[MPa]$ | 52900 |
| Ultimate tensile strength $[MPa]$ | 690 |
| Yield strength $[MPa]$ | 690 |
| Density $[kg/m^3]$ | 1535 |
| Percentage elongation at the ultimate point (point break) | $1-2\%$ |

Table 15: Main features of CARBON/EPOXY T300/934.

### 4.4.1 Cylindrical tank with ellipsoidal shells

For the last time, a cylindrical tank with an ellipsoidal shell is considered in this first case. The geometries calculated with CARBON/EPOXY T300/934 are expected to give the best results. This is because Carbon Fibre composites are among the newest and most innovative materials that can be found in the aerospace field. The results found for the following geometries before the optimization of the same were already comparable with the results found for the same geometries, with the previous materials, before the optimizations. Consequently, the post-optimization values will be decidedly higher than those relating to the previous materials, and, after the optimization, the code has calculated the new inputs that are:

1. Ullage Volume, equal to $0.37\,m^3$;
2. Micture Ratio, $\alpha = 1.74$.

In the first column of the following table is reported the performance evaluated with the input parameters of the reference case [7], i.e. the one reported in Section 3.2.1, considering the cylindrical tank with ellipsoidal shells made in CARBON/EPOXY T300/934 (Ell-C/E) [9], [10], [14]. On the other hand, the second column reports the launcher characteristic and performance for the optimized design obtained for the same material/geometry combination. The values obtained from the reference case, on the other hand, were presented in section 1 of the third chapter, and therefore are not reported here.

| | Symbols | Initial results | Post-Optimization results |
|---|---|---|---|
| Propellant mass $[kg]$ | $m_{prop}$ | 440.4 | 437 |
| Fuel mass $[kg]$ | $m_{fuel}$ | 138.7 | 141 |
| Oxidiant mass $[kg]$ | $m_{ox}$ | 301.7 | 296 |
| Pressurizing gas mass $[kg]$ | $m_{gas}$ | 1.1 | 1.7 |
| Total mass of the tank $[kg]$ | $m_{tank}$ | 1.1 | 1.4 |
| Combustion chamber mass $[kg]$ | $m_{cc}$ | 9 | 9.4 |
| Nozzle mass $[kg]$ | $m_{nozzle}$ | 10.4 | 9.3 |
| Mass of the case $[kg]$ | $m_{case}$ | 20.6 | 23.2 |
| Liner mass $[kg]$ | $m_{lin}$ | 0.9 | 1.1 |
| Dry Mass 1 $[kg]$ | $m_{dry1}$ | 258.4 | 276 |
| Dry Mass 2 $[kg]$ | $m_{dry2}$ | 129.2 | 138 |
| Dry Mass 3 $[kg]$ | $m_{dry3}$ | 43.1 | 46 |
| Tank volume $[m^3]$ | $V_{tank}$ | 0.52 | 0.63 |
| Tank radius $[m]$ | $r_{tank}$ | 0.24 | 0.26 |
| Rocket's diameter $[m]$ | $D_{rocket}$ | 0.49 | 0.51 |
| Thickness of the tank $[mm]$ | $s_{tank}$ | 0.14 | 0.15 |
| Combustion chamber thickness $[mm]$ | $s_{case}$ | 0.04 | 0.05 |
| Liner thickness $[mm]$ | $s_{lin}$ | 0.16 | 0.16 |
| Tank lenght $[m]$ | $l_{tank}$ | 3.1 | 3.4 |
| Nozzle lenght $[m]$ | $L_{nozzle}$ | 0.6 | 0.6 |
| Rocket's total lenght $[m]$ | $L_{rocket}$ | 4.9 | 5.2 |
| Payload mass $[kg]$ | $m_{payload}$ | 80 | 85.5 |
| Final mass (payload+dry) $[kg]$ | $m_F$ | 123 | 131.5 |

Table 16: Ell-C/E

Analyzing the values in the table, it is immediately evident how the thicknesses are closer to those of materials such as Dural. Compared to Dural, however, it has higher values of resistance to efforts. Therefore, what is obtained is a material-geometry combination that has both low weights and high mechanical performances. This is to the detriment of an almost absent plastic deformation capacity. Therefore, careful analysis and precautions would be necessary to predict the behaviour of this material with these geometries and, for example, remove the piece or carry out maintenance on it before it gets too close to the breaking stress values. For this first geometry, a percentage increment of approximately $6,9\%$ of the payload mass is obtained compared to the pre-optimization value. This percentage is a good value as can be seen in the summary table at the end of the subsection.

### 4.4.2 Cylindrical tank with spherical shells

In this second case, a cylindrical tank with spherical shells is considered. Also in this case the initial input parameters and the process used in the new version of the code have been defined in the previous chapter and therefore will not be reported here. Instead, the following are the new input parameters and the main quantities obtained from the optimization. The geometries calculated with CARBON/EPOXY T300/934 are expected to give the best results. This is because Carbon Fibre composites are among the newest and most innovative materials that can be found in the aerospace field. The results found for the following geometries before the optimization of the same were already comparable with the results found for the same geometries, with the previous materials, before the optimizations. Consequently, the post-optimization values will be decidedly higher than those relating to the previous materials, after the optimization, the code has found out the optimal design, which are:

1. Ullage volume, $V_{g_i} = 0.36\,m^3$;
2. Mixture ratio, $\alpha = 1.75$.

In the first column of the following table is reported the performance evaluated with the input parameters of the reference case [7], i.e. the one reported in Section 3.2.2, considering the cylindrical tank with spherical shells made in CARBON/EPOXY T300/934 (Sp-C/E) [9], [10], [14]. On the other hand, the second column reports the launcher characteristic and performance for the optimized design obtained for the same material/geometry combination. The values obtained from the reference case, on the other hand, were presented in section 1 of the third chapter, and therefore are not reported here.

| | Symbols | Initial results | Post-Optimization results |
|---|---|---|---|
| Propellant mass $[kg]$ | $m_{prop}$ | 440.2 | 436.8 |
| Fuel mass $[kg]$ | $m_{fuel}$ | 138.7 | 140.6 |
| Oxidiant mass $[kg]$ | $m_{ox}$ | 301.5 | 296.3 |
| Pressurizing gas mass $[kg]$ | $m_{gas}$ | 1.1 | 1.6 |
| Total mass of the tank $[kg]$ | $m_{tank}$ | 1 | 1.2 |
| Combustion chamber mass $[kg]$ | $m_{cc}$ | 9 | 9.3 |
| Nozzle mass $[kg]$ | $m_{nozzle}$ | 10.4 | 9.4 |
| Mass of the case $[kg]$ | $m_{case}$ | 20.1 | 22.5 |
| Liner mass $[kg]$ | $m_{lin}$ | 1.8 | 2.1 |
| Dry Mass 1 $[kg]$ | $m_{dry1}$ | 260.1 | 277.3 |
| Dry Mass 2 $[kg]$ | $m_{dry2}$ | 130.1 | 138.6 |
| Dry Mass 3 $[kg]$ | $m_{dry3}$ | 43.4 | 46.2 |
| Tank volume $[m^3]$ | $V_{tank}$ | 0.52 | 0.62 |
| Tank radius $[m]$ | $r_{tank}$ | 0.24 | 0.25 |
| Rocket's diameter $[m]$ | $D_{rocket}$ | 0.48 | 0.51 |
| Thickness of the tank $[mm]$ | $s_{tank}$ | 0.14 | 0.15 |
| Combustion chamber thickness $[mm]$ | $s_{case}$ | 0.04 | 0.05 |
| Liner thickness $[mm]$ | $s_{lin}$ | 0.15 | 0.15 |
| Tank lenght $[m]$ | $l_{tank}$ | 2.5 | 2.7 |
| Nozzle lenght $[m]$ | $L_{nozzle}$ | 0.6 | 0.6 |
| Rocket's total lenght $[m]$ | $L_{rocket}$ | 4.8 | 5.1 |
| Payload mass $[kg]$ | $m_{payload}$ | 79.6 | 84.6 |
| Final mass (payload+dry) $[kg]$ | $m_F$ | 122.9 | 130.8 |

Table 17: Sp-C/E

Analyzing the values in the table, it is immediately evident how the thicknesses are closer to those of materials such as Dural. Compared to Dural, however, it has higher values of resistance to efforts. Therefore, what is obtained is a material-geometry combination that has both low weights and high mechanical performances. This is to the detriment of an almost absent plastic deformation capacity. Therefore, careful analysis and precautions would be necessary to predict the behaviour of this material with these geometries and, for example, remove the piece or carry out maintenance on it before it gets too close to the breaking stress values. For this first geometry, a percentage increment of approximately

$6,4\%$ of the payload mass is obtained compared to the pre-optimization value. This percentage is a good value as can be seen in the summary table at the end of the subsection.

### 4.4.3 Cylindrical tank with truncated cone shells

Finally, a cylindrical tank with truncated cone shells is considered in this third case. The initial input parameters and the process used in new version of the code is being defined in the previous Chapter and so they will not be reported here. Instead, the new optimal design and the main quantities obtained from the optimization are shown below. The geometries calculated with CARBON/EPOXY T300/934 are expected to give the best results. This is because Carbon Fibre composites are among the newest and most innovative materials that can be found in the aerospace field. The results found for the following geometries before the optimization of the same were already comparable with the results found for the same geometries, with the previous materials, before the optimizations. Consequently, the post-optimization values will be decidedly higher than those relating to the previous materials, and after the optimization, the code has found out the optimal design, which are:

1. Ullage volume equal to $V_{g_i} = 0.37\,m^3$;
2. Mixture ratio equal to $\alpha = 1.74$.

In the first column of the following table is reported the performance evaluated with the input parameters of the reference case [7], i.e. the one reported in Section 3.2.3, considering the cylindrical tank with truncated cone shells made in CARBON/EPOXY T300/934 (Tc-C/E) [9], [10], [14]. On the other hand, the second column reports the launcher characteristic and performance for the optimized design obtained for the same material/geometry combination. The values obtained from the reference case, on the other hand, were presented in section 1 of the third chapter, and therefore are not reported here.

| | Symbols | Initial results | Post-Optimization results |
|---|---|---|---|
| Propellant mass $[kg]$ | $m_{prop}$ | 441.1 | 437.7 |
| Fuel mass $[kg]$ | $m_{fuel}$ | 138.9 | 141.1 |
| Oxidiant mass $[kg]$ | $m_{ox}$ | 302.2 | 296.5 |
| Pressurizing gas mass $[kg]$ | $m_{gas}$ | 1.1 | 1.7 |
| Total mass of the tank $[kg]$ | $m_{tank}$ | 1.2 | 1.5 |
| Combustion chamber mass $[kg]$ | $m_{cc}$ | 9 | 9.4 |
| Nozzle mass $[kg]$ | $m_{nozzle}$ | 10.4 | 9.3 |
| Mass of the case $[kg]$ | $m_{case}$ | 19.5 | 22.1 |
| Liner mass $[kg]$ | $m_{lin}$ | 1 | 1.2 |
| Dry Mass 1 $[kg]$ | $m_{dry1}$ | 253.4 | 270.8 |
| Dry Mass 2 $[kg]$ | $m_{dry2}$ | 126.7 | 135.4 |
| Dry Mass 3 $[kg]$ | $m_{dry3}$ | 42.2 | 45.1 |
| Tank volume $[m^3]$ | $V_{tank}$ | 0.51 | 0.62 |
| Tank radius $[m]$ | $r_{tank}$ | 0.24 | 0.25 |
| Rocket's diameter $[m]$ | $D_{rocket}$ | 0.48 | 0.5 |
| Thickness of the tank $[mm]$ | $s_{tank}$ | 0.14 | 0.15 |
| Combustion chamber thickness $[mm]$ | $s_{case}$ | 0.04 | 0.05 |
| Liner thickness $[mm]$ | $s_{lin}$ | 0.14 | 0.15 |
| Tank lenght $[m]$ | $l_{tank}$ | 2.9 | 3.1 |
| Nozzle lenght $[m]$ | $L_{nozzle}$ | 0.6 | 0.6 |
| Rocket's total lenght $[m]$ | $L_{rocket}$ | 4.8 | 5 |
| Payload mass $[kg]$ | $m_{payload}$ | 81.8 | 87.2 |
| Final mass (payload+dry) $[kg]$ | $m_F$ | 124 | 132.3 |

Table 18: Optimization of Cylindrical tank with truncated cone shells made in Carbon Fibre.

Analyzing the values in the table, it is immediately evident how the thicknesses are closer to those of materials such as Dural. Compared to Dural, however, it has higher values of resistance to efforts. Therefore, what is obtained is a material-geometry combination that has both low weights and high mechanical performances. This is to the detriment of an almost absent plastic deformation capacity. Therefore, careful analysis and precautions would be necessary to predict the behaviour of this material with these geometries and, for example, remove the piece or carry out maintenance on it before it gets too close to the breaking stress values. For this first geometry, a percentage increment of approximately

6, 56% of the payload mass is obtained compared to the pre-optimization value. This percentage is a good value as can be seen in the summary table at the end of the subsection. Also, the post-optimization payload mass value is much higher than the previous values. This implies that this will be the best geometry in conjunction with what theory already appears to be one of the best-performing materials on the market. Therefore, this pair will be the one used to obtain the results and graphs necessary for the completion of the thesis work. The optimum pair was therefore found among all those available.

## 4.5 Summary tables of main quantities

The following table will compare the values of the payload masses for each geometry-material pair. Through this comparison, the percentage variations of these masses will be calculated using the following formula

$$PercentageChange = \frac{(Final_{payload} - Initial_{payload})}{Initial_{payload}} \bullet 100 \tag{69}$$

| Geometry-Material | Initial result | Post-Optimization result | Percentage variation (increment) |
|---|---|---|---|
| Ref-All | 48.1 | 48.1 | – |
| Ell - Ti | 75.5 | 79.7 | 5.6% |
| Sp - Ti | 73.3 | 76.8 | 4.7% |
| Tc - Ti | 76.8 | 80.7 | 5.1% |
| Ell - Du | 72 | 75.4 | 4.7% |
| Sp - Du | 68.5 | 71.1 | 3.8% |
| Tc - Du | 73 | 76.1 | 4.2% |
| Ell - Inc | 73.5 | 77.3 | 5.1% |
| Sp - Inc | 70.6 | 73.6 | 4.1% |
| Tc - Inc | 74.7 | 78.1 | 4.6% |
| Ell - C/E | 80 | 85.5 | 6.9% |
| Sp - C/E | 79.6 | 84.6 | 6.4% |
| Tc - C/E | 81.8 | 87.2 | 6.6% |

Table 19: Summary of payload mass variations.

As we can see from the values in the table, the Reference case [7] already started from an optimized situation and consequently, the percentage variation cannot be calculated. Despite this, the value of the payload mass calculated in this case has been entered, so that the differences with the new cases presented in this thesis are evident. Among the various comparative analyzes that can be done, the most interesting ones are:

1. Comparison between the Reference case and the similar one, i.e. the cylindrical tank with shperical shells made in Dural: as previously mentioned, these two cases differ in some improvements made to the new version of the code and in the material, which in the new case will be the Dural, while in the reference case it was a generic Aluminium alloy. These changes result in a shift of the calculated payload mass from $48.1\,kg$ to $71.1\,kg$, i.e. a percentage change of 47.8%. Such a high percentage improvement is given by the fact that the thicknesses, in the new version of the code, are calculated and not imposed. Consequently, the calculated values are particularly small as mentioned in section 4.1.1. Consequently, not being certain of the effective realization of such small thicknesses, the effective value of the percentage increase in mass of the Payload, with respect to the case of Reference [7], will certainly be lower than the one mentioned above. So, the percentage gain in terms of payload mass will be lower than above.

2. Comparison between the Reference case and the cylindrical tank with ellipsoidal shells made in Carbon Fibre: after the comparison made in the previous point, in which the new comparison geometry was not particularly performing, we move on to the comparison between the reference case and one of the two most interesting cases, namely that of the cylindrical tank with ellipsoidal caps made of carbon fiber . In this case, a fairly high percentage increase value of the payload mass is expected, since both the material and the geometry in question are very performing. In this second comparison, the payload mass shift from $48.1\,kg$ to $85.5\,kg$ with a percentage change of 77.8%. Also in this case, the percentage gain is very high. This is linked to the considerations made in the previous point, concerning the effective realization of very thin thicknesses, such as those presented in Table 17. In any case, even if the percentage gain will be lower, there will still be improvements connected to the transition to a very thin material performing, which is the CYCOM 934, combined with the use of a different geometry.

3. Comparison between the Reference case and the cylindrical tank with truncated cone shells made in Carbon Fibre: this last case shows the reference case compared with the most interesting case, i.e. that of the cylindrical tank with truncated cone shells made of carbon fibre. This material

geometry couple is the one that allows us to obtain the best results in terms of payload mass and all subsequent analyzes will be limited to this case, always in comparison with the initial reference case. In the latter case, we pass from a payload mass value of $48.1\,kg$ for the reference case to a value of $87.2\,kg$ for the case in question, with a consequent percentage variation of 81.3%. Also in the latter case, the main advantages are connected to the lower weight of the tank, obtained using the thicknesses in Table 18. Also in this case these thicknesses have very small values and consequently it is not said that there is a production process capable of realizing such laminate. However, an effective improvement is expected since, although the real thicknesses will be greater than the calculated ones, they should be lower than those in the case of Reference [7], thanks to the fact that the new material appears to be very performing at a structural level.

Then, in the continue will be analyzed the evolution of the main quantities relating to the aforementioned couple, comparing these results with those relating to the reference case.
Another table of interest is that concerning the comparison of specific modulus values and specific strength (also named breaking length); these two quantities have been defined in section 4.1.1. Furthermore, to obtain the results of interest, the results obtained by the values in the table were divided by 9.81 to obtain the metric unit of measurement and subsequently by 1000 to obtain the unit of measurement most suited to the aforementioned values, i.e. kilometer.

| | $E$ | $\sigma_{Max}$ | $\rho_M$ | $E/\rho_M$ | $\sigma_{Max}/\rho_M$ | Unit of measure |
|---|---|---|---|---|---|---|
| All( Ref) | $73100 \bullet 10^6\,Pa$ | $392 \bullet 10^6\,Pa$ | $2800\,kg/m^3$ | 2661.3 | 14.3 | $km$ |
| Ti | $104000 \bullet 10^6\,Pa$ | $600 \bullet 10^6\,Pa$ | $4512\,kg/m^3$ | 2349.6 | 13.6 | $km$ |
| Du | $73100 \bullet 10^6\,Pa$ | $259.2 \bullet 10^6\,Pa$ | $2780\,kg/m^3$ | 2680.4 | 9.5 | $km$ |
| Inc | $200000 \bullet 10^6\,Pa$ | $880 \bullet 10^6\,Pa$ | $8190\,kg/m^3$ | 2489.3 | 11 | $km$ |
| C/E | $52900 \bullet 10^6\,Pa$ | $460 \bullet 10^6\,Pa$ | $1535\,kg/m^3$ | 3513 | 30.6 | $km$ |

Table 20: Summary of comparable useful structural parameters.

Thanks to the analysis previously carried out, and thanks to the values obtained in this table, it can be stated that the material selected for the continuation of the performance analysis, i.e. carbon fiber is certainly the best performing with a breaking length value just over double that of the material used in the Reference case[7]. Therefore, proof of the right selection with regard to the material is given, as this turns out to be the best among those tested, and it will turn out to be a totally appropriate choice from a purely structural point of view.

## 4.6 Analysis of the best solution: cylindrical tank with truncated cone shells made in Carbon Fiber Composite.

In this last section of chapter 4, the performance analysis of the best geometry-material couple is carried out. The graphs of the main quantities of interest, as a function of time, are then reported and analysed; these graphs also show the same quantities relative to the case of Reference [7] in such a way as to have proof of the fact that the results obtained with the new code are correct. The deviations that will be noticed between the two curves are the result of having changed the design of the rocket through the implementation of the new geometry-material combination.

In Figure.16 we can observe the mixture ratio ($\alpha$) as a function of time for the two cases, while in Figure.17 the specific impulse ($I_s$) as a function of time is presented. Since these two quantities are connected, analyzing them separately would risk losing useful information for the analysis of Performance.

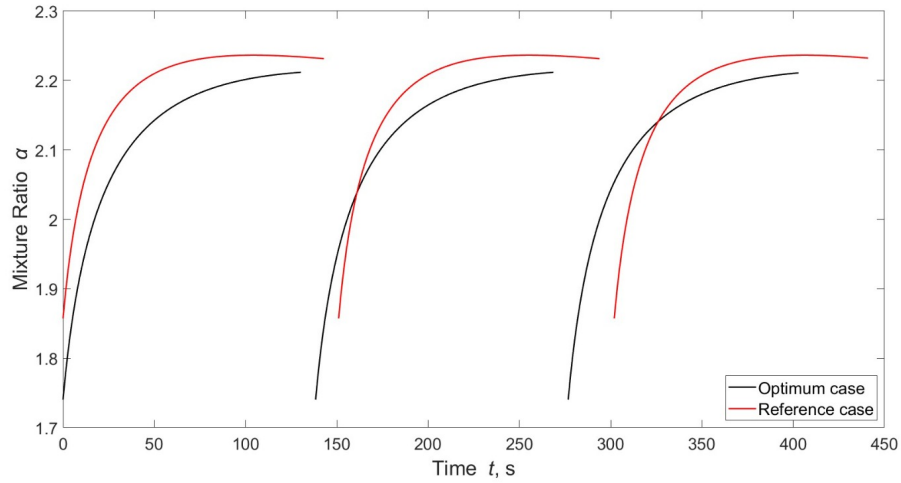


Figure 16: Mixture ratio in function of the time.

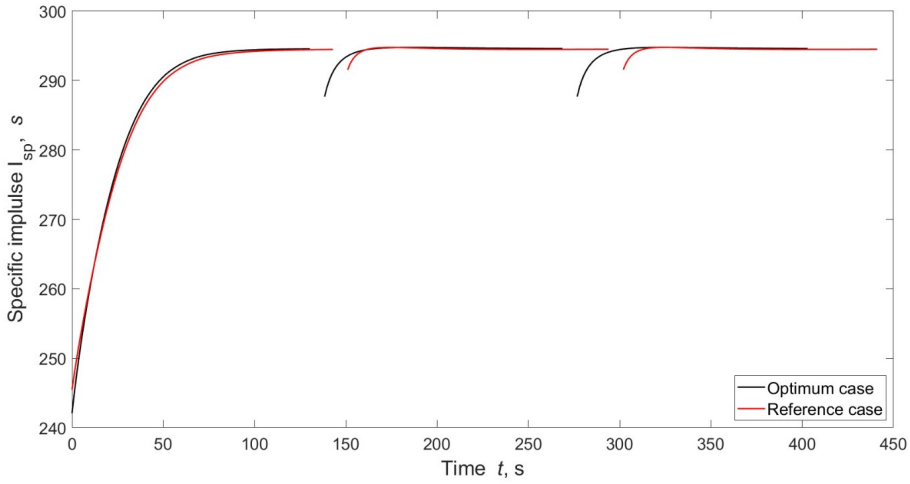


Figure 17: Specific impulse in function of the time.

In both cases, the optimization of the design involves the growth of the mixture ratio during the engine operations; the mixture ratio values grow starting from the optimum value, i.e. $\alpha = 1.86$ in the Reference case [7] and $\alpha = 1.74$ in the Optimal case. Starting from these values, the mixture ratios grow up to reach the values that maximize the specific impulse: the specific impulse and the mixture ratio, in fact, are indirectly linked and this could easily be demonstrated by developing the equations presented in section 1.1.

An increase in the mixture ratio during the mission involves an increase of the specific impulse (this is valid for alpha values less than or equal to about 3) up to the maximum value which corresponds to an $\alpha$ of 2.2 in both cases. In the first case, the maximum of the specific impulse is reached after a time of $143s$ while in the second case it is maximized after $132s$. Furthermore, from the literature [6] it is known that the optimal specific impulse value for the combustion/oxidant combination chosen for this thesis work is obtained for a mixture ratio equal to 2, and is approximately equal to $I_s = 250 - 300s$. In our case for alpha values equal to 2.2, i.e. the optimum value, we see the achievement of $I_s$ values comparable to those found in the literature [2], [15].
An increase in the specific impulse would lead to a reduction in the propellant used, but in the case under examination, having changed the design increased the quantity of propellant, with a consequent increase in the flow rate, compared to the case of Reference [7]. This leads to a reduction in the mission time for the same altitude to be reached. The increase in the specific impulse value will therefore be due to an increase in thrust, with the same initial value. Thanks to the new design, we have a higher propellant flow rate, higher thrusts, shorter mission times and overall higher specific impulses. Since the specific impulse measures how efficiently the propellant mass is used [2], [15], its increase leads us to say that the new design of the rocket is more efficient than the design of the Reference case.
Furthermore, the rocket needs acceleration values high enough for a sufficient flight time, to maintain an ascending trajectory that moves the aircraft towards the imposed orbital altitude. In addition, the aerodynamic drag values during the early flight phases are considerable, consequently, sufficiently high Thrust values will be required. To reach this, a large volume of pressurized gas is required to avoid excessive drop of pressure inside the tank which would affect the real thrust levels [7]. The choice of a sufficiently low initial mixture ratio value, in this initial phase of the mission, involves a reduction of the oxidant flow with consequent advantages for the aforementioned problem.
The two successive quantities, presented in Fig.18 and Fig.19, will also be analyzed together as they are connected; these are the Thrust and the Acceleration produced by this, as a function of time.

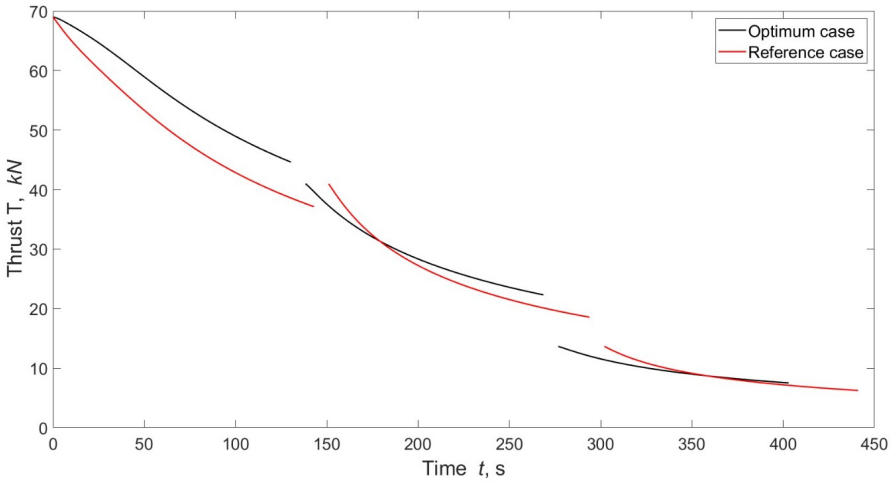


Figure 18: Thrust in function of the time.

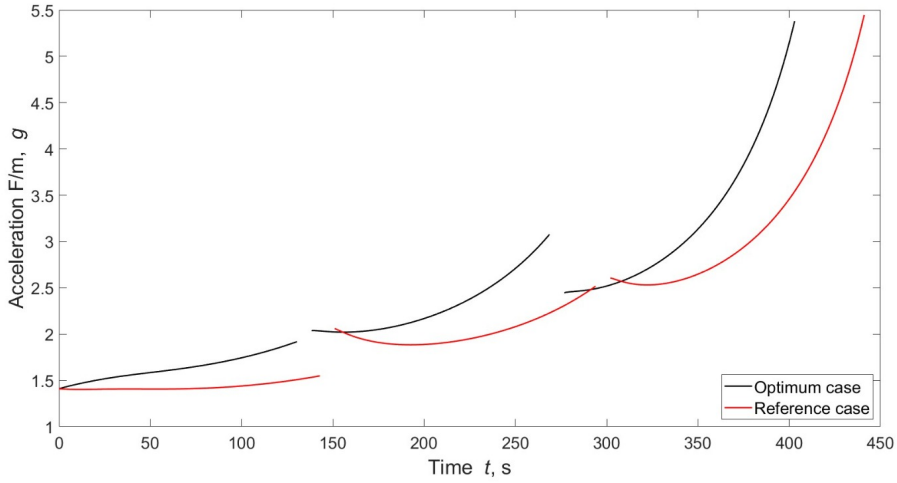


Figure 19: Longitudinal Acceleration (Thrust Acceleration) in function of the time.

Thanks to the variation of the engine design, which involves a greater mass of propellant available and therefore a greater flow rate (with the same fuel used and considering the area where the flow will pass, which has not changed excessively between the Reference case and the optimized case), it is possible to obtain a greater level of thrust during the phases of the mission, with the same initial thrust. Furthermore, as mentioned in the paper in Reference [7], the Thrust is strongly influenced by the altitude (in the atmosphere).
What has been said has direct consequences on the quantity in Fig.19: as in the case of Reference [7], one could expect that the acceleration curve presents the same trend as the thrust. This does not happen because the variation of the masses during the mission, due to the release of the components and the consumption of propellant, involves an overall increasing trend of the acceleration. The optimized case initially sees the achievement of greater acceleration values during the mission. This is given both by the trend of the thrust in Fig.18, and because the mass in the optimal case is not divided in the same way as in the Reference case: being the most performing material and therefore the lightest structure, with a consequent increase in payload mass, lighter components will be separated when released, with masses of the second and third stage greater than those of the Reference case. Consequently, the two terms will counterbalance each other less than in the case of Reference, and the overall trend will be more increasing. Finally, it can be observed that the burnout values of the final phase are relatively large and are close to $5.5 - 6\,g$, which is a typical limit in the functioning of the launcher [7].
Regarding the Regression rate, with the same geometry, this directly depends, through an exponent, on the oxidant flow. This is therefore due to the variation of the evolution of this parameter in the case of optimum, with respect to the trend of the Reference case [7].
In fact, the flow rate of the oxidant used in the case of Reference [7] turns out to be lower than that calculated in the case of Optimal, and consequently, there is a trend tending to lower values in the first case.
This quantity, as well as the mixture ratio, cannot vary arbitrarily, and for this reason, the optimization of hybrid propellant rockets is very complicated. Fig.20 allows us to notice how the trend of this quantity between the two cases considered is very similar. The greater rapidity of evolution in our case is always connected to the discussion made previously regarding the different design and the consequences this has on the propellant flow.

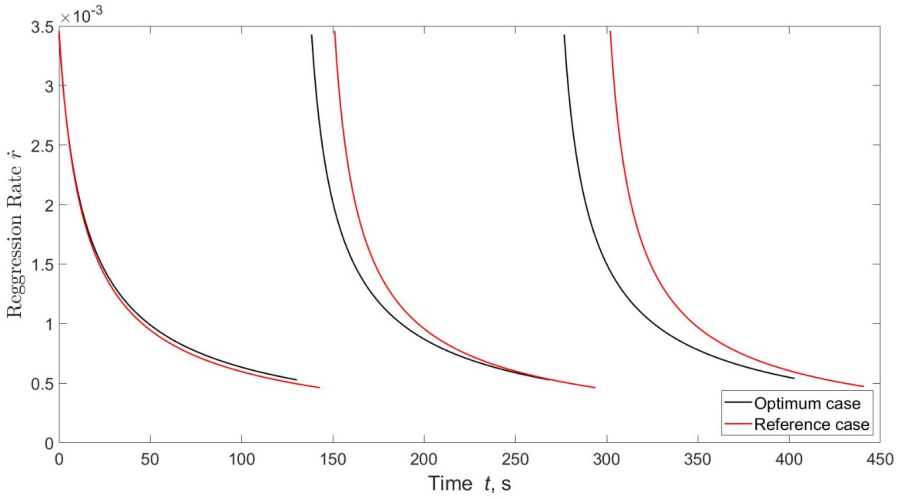


Figure 20: Regression Rate in function of the time.

Finally, the propellant flow trend during the mission is presented in Fig.21. As previously mentioned, the variation of the rocket design (which has lower dry masses and therefore a greater share of the propellant flow rate and nevertheless a good payload value) involves a variation of the propellant flow rate which in turn will lead to values of greater thrust and slightly shorter mission times. Therefore higher propellant flow rates are beneficial for rocket performance.

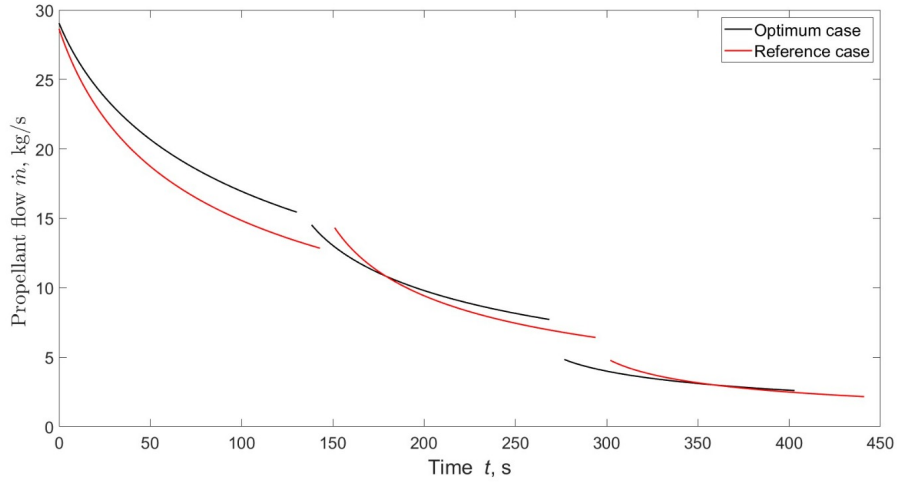


Figure 21: Propellant flow in function of the time.

# 5 Conclusions

The purpose of this thesis work was to compare other geometries and innovative materials that would bring effective improvements to the optimization process concerning the masses of a hybrid propellant rocket engine for small launchers. This objective can be considered achieved: the payload mass values found with the new geometries and with particularly performing materials turn out to be greater than the value that was calculated in the case of Reference [7]. Going beyond what has been done in this thesis, however, a consideration that catches the eye concerns the trade-off of the quantities. In fact, any design process involves a trade-off, usually multi-disciplinary, between different aspects and different dimensions.
Specifically, the main considerations on which we could focus are:

- Costs: in the vast majority of cases the project includes initial cost analyses that guide the designer in the Design choices. Consequently, it is not certain that the most performing material is selectable for a project, as the costs of it and/or the manufacturing processes connected to it could be too high.
- Effective realization of the design obtained: as previously said, very performing materials lead to very "extreme" geometries that are not always achievable. Also, in this case, an analysis of the machining process could lead to an increase in the thicknesses or sizes of the rocket and therefore it is not certain that a geometry that is better after optimization, remains so even after these considerations.

For the realization of the thesis project, we started by implementing geometries similar to that of the Reference case, but which presented shapes related to the more elaborate shells of the simple spherical shape. Subsequently, materials were introduced. Among these, there are more common ones in the aeronautical field, such as Dural, and others more particular and unusual due to the other costs and the fact that research on them is still active. Finally, the material-geometry pair was selected which gave the best overall performance.

Future developments are desirable for the construction of increasingly high-performance rockets and consequently that allow for the insertion of increasingly larger masses of payload into orbit.
Some possible future trends could investigate the possibility of changing the position of the tanks, using oxidizer tanks placed in parallel with the fuel tank and evaluating whether this configuration, which would turn out to be shorter and wider, could lead to advantages. Other changes could concern the shape of the nozzle and the introduction of innovative geometric shapes. These possible future trends, in addition to potentially improving the current version of the code, could lead to actual real improvements, if these are accompanied by multidisciplinary design analyzes.

# References

[1] Sutton, Biblarz, «Rocket Propulsion Elements», J. Wiley& Sons, Ninth Edition (2017);

[2] Appunti personali del corso «Endoreattori» tenuto da D. Pastrone(2020);

[3] Frota, Ford, «Review on Hybrid Propellants», A. Wilson, Proceedings of the 2nd International Conference on Green Propellants for Space Propulsion (ESA SP-557). 7-8 June 2004;

[4] C. Schmierer, M. Kobald, U. Fischer, «Advancing Europe's Hybrid Rocket Engine Technology with Paraffin and LOX», 8Th European Conference for Aeronautics and Aerospace Sciences (EUCASS);

[5] Makled, «Hybrid Rocket Motor: Propellant Selection and Fuel Grain Design», 8th International Conference on Chemical & Environmental Engineering (2016);

[6] Appunti personali del corso «Motori per Aeromobili» tenuto da D.Pastrone (2020);

[7] L. Casalino, F. Masseni, D.Pastrone, «Hybrid Rocket Engines for Small Satellite Launchers», Politecnico di Torino;

[8] Huzel, K. Dieter, Huang, H. David, «Modern Engineering for Design of Liquid-Propellant Rocket Engines», Published by the American Institute of Aeronautics and Astronautics, 1992

[9] F. Megyesy, «Pressure Vessel Handbook», Pressure Vessel Handbook Publishing, Twelfth Edition;

[10] TECHNICAL DATA SHEET No. CFA-001, «T300 Data Sheet», Toray Carbon Fibers America;

[11] TECHNICAL DATA SHEET, «Titanium Alloy Ti 6Al-4V», Carpenter Technology;

[12] Appunti personali del corso «Strutture Aeronautiche» tenuto da M. Di Sciuva;

[13] TECHNICAL DATA SHEET, «INCONEL Alloy 718», Special Metals;

[14] TECHNICAL DATA SHEET, «CYCOM 934 Epoxy PREPREG», Cytec;

[15] Appunti personali del corso «Propulsione spaziale» tenuto da L. Casalino;